

THE UNIVERSITY OF CALGARY

SOUND PROPAGATION UNDER TEMPERATURE

INVERSION CONDITIONS IN SOUTHERN ALBERTA

BY

DAVID ALLAN BOHLENDER

A THESIS

SUBMITTED TO THE FACULTY OF GRADUATE STUDIES

IN PARTIAL FULFILLMENT OF THE REQUIREMENTS FOR THE

DEGREE OF MASTER OF SCIENCE

DEPARTMENT OF PHYSICS

CALGARY, ALBERTA

JUNE, 1984

(C) DAVID ALLAN BOHLENDER 1984

THE UNIVERSITY OF CALGARY

FACULTY OF GRADUATE STUDIES

The undersigned certify that they have read, and recommend to the Faculty of Graduate Studies for acceptance, a thesis entitled "Sound Propagation Under Temperature Inversion Conditions in Southern Alberta," submitted by David Allan Bohlender in partial fulfillment of the requirements for the degree of Master of Science.

T. Mathews

Chairman, Dr. T. Mathews
Department of Physics

R. B. Hicks

Dr. R. B. Hicks
Department of Physics

T. K. Groves

Dr. T. K. Groves
Department of Mechanical Engineering

Date 2 Aug 84

ABSTRACT

An experimental investigation of the propagation of sound under inversion conditions has been conducted at two sites: Springbank Airport, 20 km west of Calgary, and near Vulcan, Alberta.

Flow resistivities of several surfaces have been measured by making a best fit of experimental excess attenuations of sound near the ground to theoretical expectations. Values of 60 cgs rayls for a plowed field, 30 cgs rayls for a snow covered field and 170 cgs rayls for a grass field so obtained are consistent with previously published results.

A comparison of sound levels measured during temperature inversions with intensities predicted for neutral atmospheric conditions has been made. It is found that for distances of 550 m and less from a sound source the presence of a temperature inversion causes no enhancement in the sound field near the surface.

For propagation distances of 830 m and greater enhancements of up to 25 dB relative to normal daytime conditions when a ground-based inversion was present have been observed. Elevated inversions associated with the Southern Alberta Chinook were found to occasionally enhance sound levels to a similar degree and at times cause an increase

in attenuations of up to 15 dB relative to those measured during the day.

Rapid fluctuations in the measured sound intensities of up to 35 dB were observed at distances of 1730 and 2180 m from the source when an elevated inversion was present. These effects are shown to be caused by the refractive focusing of sound by the temperature and wind gradients aloft.

Suggestions for further research are presented.

ACKNOWLEDGEMENTS

The author would like to thank the many people who contributed directly or indirectly to the preparation of this thesis:

Dr. Titus Mathews for his support, suggestions and seemingly endless patience,

Mr. Fred Babott for "Fred's Box," the description of the electronics and its specifications,

Mr. Duncan Smith for help with the ray tracing routines and their modifications and suggestions and discussions regarding this work,

Dr. R. B. Hicks for his helpful comments and never saying no to requests for more computer time,

Mr. Ted Rhodes for meteorological instruments and tables,

My valued friends, new and old, for their support, understanding and persistence; Charlene, Linda and Mrs. H., Theresa, Helena, Tim and Pradelia, Pratima and David - you were often ignored, but never forgotten,

My sister Debbie, brother Mark and sister-to-be Cindy for their encouragement, support and awe,

Of course, Mum and Dad for their worry, concern, etc., and for not throwing me back,

And the entire Irwin clan without whom much of this would have been impossible: David and Tom Irwin for their tremendous help and suggestions, Edith and Felicia for their support and meals, and last, but not least, Patrick for his ear, humour, the "Pat Irwin correction factor," reminding me I have a home, seeing that we both eat at least once a day and for a lasting friendship.

To Charlene

"It's just Atmospheric Physics!"

You'll never know how much you helped
(or at least you'll never admit it).

D.

TABLE OF CONTENTS

	PAGE
ABSTRACT	iii
ACKNOWLEDGEMENTS	v
TABLE OF CONTENTS	viii
LIST OF TABLES	x
LIST OF FIGURES	xi
I. <u>OUTDOOR SOUND PROPAGATION</u>	1
1.1 Introduction	1
1.2 The Nature of Sound	5
1.3 Sound Propagation in a Free Field	8
1.4 Sound Propagation Above a Surface	11
1.5 Meteorological Effects	24
II. <u>EXPERIMENTAL EQUIPMENT AND PROCEDURE</u>	33
2.1 Overview of Equipment	33
2.2 Receiver	33
2.3 Transmitter	37
2.4 Calibration	39
2.5 Data Reduction	40
2.6 Experimental Procedure	41
III. <u>GROUND IMPEDANCE</u>	44
3.1 Review	44
3.2 Field Measurements of Ground Impedance ...	48

3.3 Experimental Results	50
IV. SOUND PROPAGATION DURING INVERSION CONDITIONS:	
EXPERIMENTAL RESULTS	54
4.1 Summary of Data	54
4.2 The Ground-based Inversion: Close-range Effects on the Propagation of Sound	56
4.3 The Effect of Temperature Inversions on the Long-range Propagation of Sound	59
4.4 The Nocturnal Inversion	65
4.5 The Elevated Inversion	69
V. SUMMARY AND DISCUSSION	83
5.1 Summary	83
5.2 Discussion	87
5.3 Suggestions for Future Work	92
BIBLIOGRAPHY	95
APPENDIX A. Effects of Atmospheric Turbulence on the Interference of Sound Waves	100

LIST OF TABLES

<u>TABLE</u>	<u>TITLE</u>	<u>PAGE</u>
3.1.1.	Flow resistivities of various ground surfaces	47
4.1.1.	Data acquistion times, durations and locations	55

LIST OF FIGURES

<u>FIGURE</u>	<u>TITLE</u>	<u>PAGE</u>
1.1.1.	Percentage of time inversions are present ...	3
1.4.1.	Source-receiver geometry for propagation of sound above a surface	13
1.4.2.	Angles of integration for equation 1.4.10 ...	18
1.4.3.	Contours of integration	18
1.4.4.	Theoretical excess attenuations for various source-receiver separations and heights and flow resistivities	23
1.5.1.	Theoretical ray paths for different meteorological conditions	27
1.5.2.	Comparison of measured sound levels with values predicted by coherent theory and turbulent theory	32
2.1.1.	Schematic of electronics	34
3.1.1.	Experimental values of the normalized specific normal impedance of grass-covered ground	47
3.3.1.	Measured and best fit theoretical excess attenuations to determine the flow resistivity	51
4.2.1.	Measured and theoretical excess attenuations: Springbank site	57
4.2.2.	Measured and theoretical excess attenuations: Springbank site	57
4.3.1.	Monostatic SODAR records of ground inversions, thermal plumes and elevated inversions	60
4.3.2.	Histogram of excess attenuations for various meteorological conditions	61

4.4.1.	Measured and theoretical excess attenuations: Vulcan site	66
4.4.2.	SODAR record and measured excess attenuations for nocturnal inversion of March 3, 1984	68
4.5.1.	SODAR record of chinook event of March 1-2, 1984	70
4.5.2.	Measured excess attenuations for chinook event of March 1-2, 1984	71
4.5.3.	Ray diagram and theoretical excess attenuations from tethersonde data at 15:40 MST March 1, 1984	73
4.5.4.	Ray diagram and theoretical excess attenuations from tethersonde data at 3:30 MST March 2, 1984	75
4.5.5.	Ray diagram for artificially raised chinook layer of March 2, 1984	76
4.5.6.	SODAR records of elevated inversion events of March 4 and 19-20, 1984	78
4.5.7.	Measured excess attenuations for elevated inversion events of March 4 and 19-20, 1984	78
4.5.8.	Ray diagram and theoretical excess attenuations from tethersonde data at 00:30 MST March 20, 1984	80
4.5.9.	Ray diagram and theoretical excess attenuations from tethersonde data at 3:30 MST March 20, 1984	81
5.2.1.	Theoretical ray paths for different inversion heights	89

CHAPTER I

OUTDOOR SOUND PROPAGATION

1.1 Introduction

The propagation of sound in the atmosphere is an extremely complex problem and in recent years the topic has received an increasing amount of attention from scientists throughout the world. In particular, interest in the propagation of sound close to a ground surface has produced a plethora of articles, both theoretical and experimental, in the scientific literature. These have included papers concerned with the effects of the ground surface on measured sound intensities (Embleton et al, 1976a and references therein), the acoustical properties of these surfaces themselves (Delany and Bazley, 1970a), meteorological effects on acoustic wave propagation (Parkins and Scholes, 1964 and 1965; Chessel, 1978; Embleton et al, 1976b; Piercy et al, 1977 and references therein), as well as complications arising from inhomogeneities or turbulence in the atmosphere (Daigle et al, 1978; Daigle, 1979). This thesis will concern itself primarily with these meteorological phenomena and in particular with the effect of a temperature inversion on the measured intensities of sound.

In Calgary, Alberta, two types of temperature inversions occur:

1. The familiar ground-based nocturnal inversion which forms after sunset when radiative cooling of the ground takes place and persists well into daylight hours.
2. The elevated inversions associated with the Southern Alberta Chinook.

The nocturnal inversion's strength, height and duration depend on the winds, cloud cover and humidity among other factors and are highly variable. Typical temperature gradients are $1.5^{\circ}\text{C}/100\text{ m}$.

In chinooks, warm westerly winds flowing over the Rocky Mountains create an interface with the cold arctic air mass below and can lead to temperature gradients as large as $30^{\circ}\text{C}/100\text{ m}$. This inversion layer often descends to the ground and may last from a few hours to several days.

The Physics Department at the University of Calgary has operated monostatic acoustic sounders since 1976 allowing for a statistical analysis of the occurrences and durations of inversions in the area, both ground-based and aloft (Mathews, 1982). Figure 1.1.1 indicates that inversions are present for about 55% of the time during summer months and approximately 85% of the time in the winter.

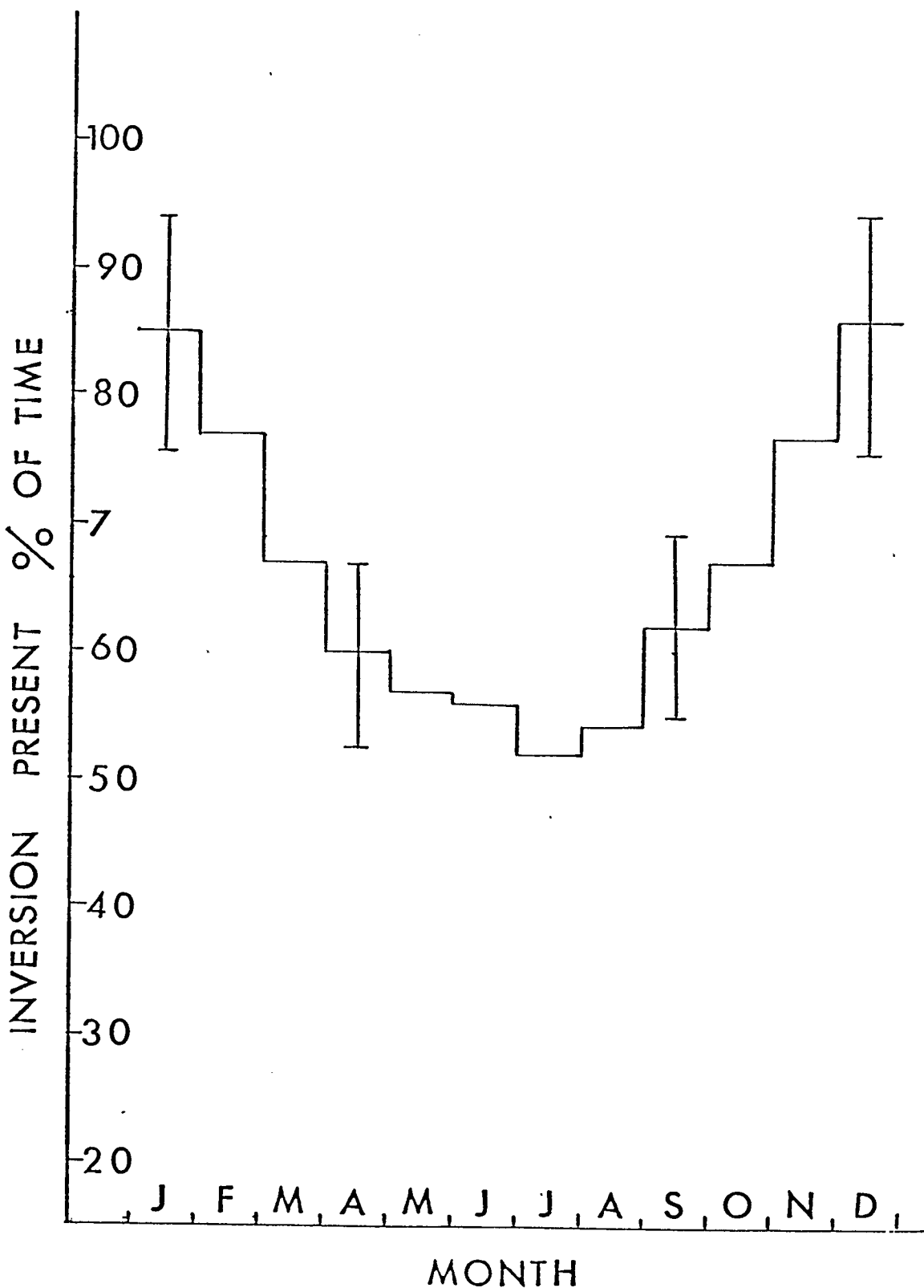


Figure 1.1.1. Percentage of time inversions are present

The increase during winter is attributable to the increased number of elevated inversions caused by chinook winds as well as the decreased hours of sunlight. Unfortunately, acoustic sounders (SODAR) give information concerning the height and depth of inversions but none regarding the temperature gradient associated with it. Temperature and wind data must be acquired by the use of a radiosonde.

Obviously the Calgary locale is well-suited for investigations into temperature inversions and their effect on sound propagation. In this work three related studies have been carried out. First the effect of the chinook on measured sound levels at the surface was explored.

In addition, an investigation was made into the propagation of sound during nocturnal inversions. In this case of near-grazing incidence of sound waves with the surface, the ground effect complicates matters considerably. Knowledge of the acoustical properties of the surface is vital to make predictions of sound levels possible, not only in normal temperature lapse conditions, but especially under inversion conditions. As a result, measurements have also been made of the acoustical impedance of several surface types to aid the theoretical investigations.

The increased concern in urban noise control demands improved predictions of sound levels and the fact that temperature inversions can significantly enhance noise levels kilome-

ters from a source make this and future studies take on special significance.

1.2 The Nature of Sound

Before beginning a discussion of the propagation of sound under temperature inversion conditions several fundamental definitions and relations will be required.

Sound is a form of radiant energy that is transmitted by longitudinal pressure waves in an elastic material at a velocity characteristic of that medium. For normal speech pressure variations are small; at a distance of one meter from the speaker they average about 0.1 N/m^2 above and below the normal atmospheric pressure at sea level ($1.013 \times 10^5 \text{ N/m}^2$) (Beranek, 1971).

In an ideal gas the speed of sound is given by

$$c = (\gamma p / \rho)^{\frac{1}{2}} \quad 1.2.1$$

where γ is the ratio of the specific heat of the gas at constant pressure to the specific heat at constant volume, p is the total pressure and ρ is the gas density. Using the equation of state for an ideal gas

$$c = 20.05\sqrt{T} \text{ m/s} \quad 1.2.2$$

where T is the temperature in Kelvins.

Associated with the sound pressure is the particle velocity, u , a measure of the motion of the air molecules along a line parallel to the direction of propagation.

For plane acoustic waves

$$u = p/\rho c \quad 1.2.3$$

Note here that u and c are two different velocities, the particle velocity and the speed of sound respectively.

The sound intensity, I , in W/m^2 , is

$$I = \overline{pu} = p_{\text{rms}}^2 / \rho c \quad 1.2.4$$

where the overbar denotes the time average and p_{rms}^2 is the mean-square sound pressure.

The specific acoustic impedance, Z , is defined to be the ratio of the sound pressure at a point to the particle velocity at that point. The unit is the Ns/m^2 or cgs rayl.

That is

$$Z = p/u \quad 1.2.5$$

For plane waves equations 1.2.3 and 1.2.5 give

$Z = \rho c = 406$ mks rayls at room temperature and pressure.

In general, however, the time-dependences of p and u are different. In this case Z is a complex quantity:

$$Z = R + iX = |Z|e^{i\psi} \quad 1.2.6$$

where ψ is the phase difference between the sound pressure and particle velocity. The real part of the impedance is called the resistance, the complex component the reactance. The analogy to electrical impedance is obvious. It will also prove convenient at the boundary between air and a denser medium to define a normal specific acoustic impedance, Z_n , as

$$Z_n = p/u_n \quad 1.2.7$$

where u_n is the component of the particle velocity normal to the plane between the two media.

Sound intensities range over a factor of more than 10^{20} . Obviously, logarithmic scales are needed to make meaningful measurements possible. The two most frequently used are the Sound Intensity Level (SIL) and Sound Pressure Level (SPL).

$$SIL = 10\log_{10}(I/I_{ref}) ; SPL = 20\log_{10}(p/p_{ref}) \quad 1.2.8$$

Usually $I_{ref} = 10^{-12}$ watts/m² and $p_{ref} = 2 \times 10^{-5}$ N/m².

For most noise measurements $SPL \approx SIL$ (Beranek, 1971) so any measured sound levels may simply be referred to as SPL's.

1.3 Sound Propagation in a Free Field

There are two effects evident in the propagation of sound in the absence of any boundaries: geometric spreading and atmospheric absorption of sound.

Assuming that an ideal point source emits W watts of acoustic power then at a distance r_1 from the source the measured SPL relative to a standard reference will be

$$SPL(r_1) = 10\log_{10} \left\{ \frac{W/4\pi r_1^2}{I_{ref}} \right\} \text{ dB} \quad 1.3.1$$

and at a distance r_2

$$SPL(r_2) = 10\log_{10} \left\{ \frac{W/4\pi r_2^2}{I_{ref}} \right\} \text{ dB} \quad 1.3.2$$

The difference in these two levels will be

$$\Delta SPL = 20\log_{10}(r_1/r_2) \text{ dB} \quad 1.3.3$$

Thus, for every doubling of the distance from a point source the SPL drops by approximately 6 dB. Similarly, it could be shown that for a line source the corresponding drop per doubling of distance would be 3 dB. Loss-free propagation would occur for an infinite area source. In practice, finite size surfaces have a nearfield where the latter is true and a farfield where the expansion is spherical.

This is an ideal approximation. In the real atmosphere absorption effects are also present. Absorption of sound is most strongly influenced by the composition of the air, most notably the water vapour content, the temperature and the frequency of the acoustic wave.

Absorption effects cause pressure to decrease exponentially according to the relation

$$p = p_0 e^{-\alpha r} \quad 1.3.4$$

where α is the absorption coefficient measured in nepers per meter and r is the propagation distance in meters.

Note that one neper is 8.69 dB so that

$$\Delta SPL = -8.69\alpha r \text{ dB} \quad 1.3.5$$

There are several different mechanisms of absorption. These include the classical absorption caused by transport processes of classical physics such as shear viscosity, thermal conductivity, mass diffusion and thermal diffusion and the rotational and vibrational relaxation of oxygen and nitrogen molecules.

The viscous losses result from the relative motion occurring between various portions of the medium during the successive expansions and contractions that accompany a propagating sound wave.

Heat conduction losses are a result of the adiabatic pressure changes occurring in the medium through which the sound wave travels. Heat is conducted from regions of compression where the temperature is raised to regions of rarefaction where the temperature is lowered. This reduces the amplitude of the wave during its propagation.

The relaxation processes cause an attenuation of the amplitude of the sound wave because of the finite times required by the molecules to adjust to changes in translational energy. For example, if compressional energy is absorbed into an internal vibration mode, the associated time lag may result in this energy being restored to the medium during a time of rarefaction and result in an overall reduction in the amplitude of the wave (Kinsler and Frey, 1962; ANSI Standard S1.26-1978).

The absorption is usually listed as an absorption coefficient, α , in units of dB/100 m (ANSI Standard S1.26-1978) and is given by

$$\alpha = f^2 \left[1.84 \times 10^{-11} \left(\frac{p_{so}}{p_s} \right) \left(\frac{T}{T_o} \right)^{\frac{1}{2}} + \left(\frac{T}{T_o} \right)^{-5/2} \right. \\ \left. \times \left\{ 1.278 \times 10^{-2} \left[\exp(-2239.1/T) \right] / \left(f_{r,0} + (f^2/f_{r,0}) \right) \right. \right. \\ \left. \left. + 1.068 \times 10^{-1} \left[\exp(-3352/T) \right] / \left(f_{r,N} + (f^2/f_{r,N}) \right) \right\} \right] \quad 1.3.6$$

where

$$f_{r,0} = (p_s/p_{so}) \{24 + 4.41 \times 10^4 h [(0.05 + h)/(0.391 + h)]\} \text{ Hz}$$

1.3.7

$$f_{r,N} = (p_s/p_{so}) (T/T_o)^{-1/2} (9 + 350h \exp\{-6.142[(T/T_o)^{-1/3} - 1]\}) \text{ Hz}$$

Here p_s is the atmospheric pressure (kPa),
 $p_{so} = 101.325 \text{ kPa (1 atm.)}$, T is the temperature (K),
 $T_o = 293.15 \text{ K}$, f is the frequency (Hz), $f_{r,0}$ and $f_{r,N}$ are
the vibrational relaxation frequencies of oxygen and
nitrogen respectively (Hz) and h is the molar concentration
of water vapour in per cent.

Other transient atmospheric constituents such as rain
and fog appear to have a negligible effect on the total absorption
of sound (Ingard, 1953; Rudnick, 1957).

1.4 Sound Propagation Above a Surface

The presence of a boundary near a sound source adds considerable interest and complexity to the study of the propagation of sound. Since most noise sources are in close proximity to the ground an understanding of the ground effect is of considerable importance.

The problem to be considered is that of the propagation of a spherical wave due to a point source S located at height h_s above a plane surface at $z = 0$ and of angular frequency $\omega = 2\pi f = kc$, in a medium of density ρ and

sound speed c . A value for the field, ϕ , is desired at the receiver R situated at a height h_r above the boundary as depicted in figure 1.4.1.

The answer will be a solution of the wave equation

$$(\nabla^2 + k^2)\phi = 0 \quad 1.4.1$$

subject to the boundary conditions at $z = 0$:

$$\rho\phi|_{z=0} = \rho_2\phi_2|_{z=0} \quad \frac{\partial\phi}{\partial z}|_{z=0} = \frac{\partial\phi_2}{\partial z}|_{z=0} \quad 1.4.2$$

These equations are equivalent to requiring that the pressure and normal components of the velocity be continuous at the boundary of the two media.

The pressure and particle velocity are given by

$$p = -\frac{\partial\phi}{\partial t} = i\rho\omega\phi \quad u = \nabla\phi \quad 1.4.3$$

so that ϕ is often called the velocity potential.

Throughout this analysis a time dependance of $e^{-i\omega t}$ is assumed for ϕ , ρ is the mass density and k_2 is the propagation coefficient in the lower medium.

First, consider the simple case of the reflection of a plane wave at the surface.

Using Snell's well known refraction law

$$k \sin\theta = k_2 \sin\eta \quad 1.4.4$$

it is easy to show that the plane wave reflection

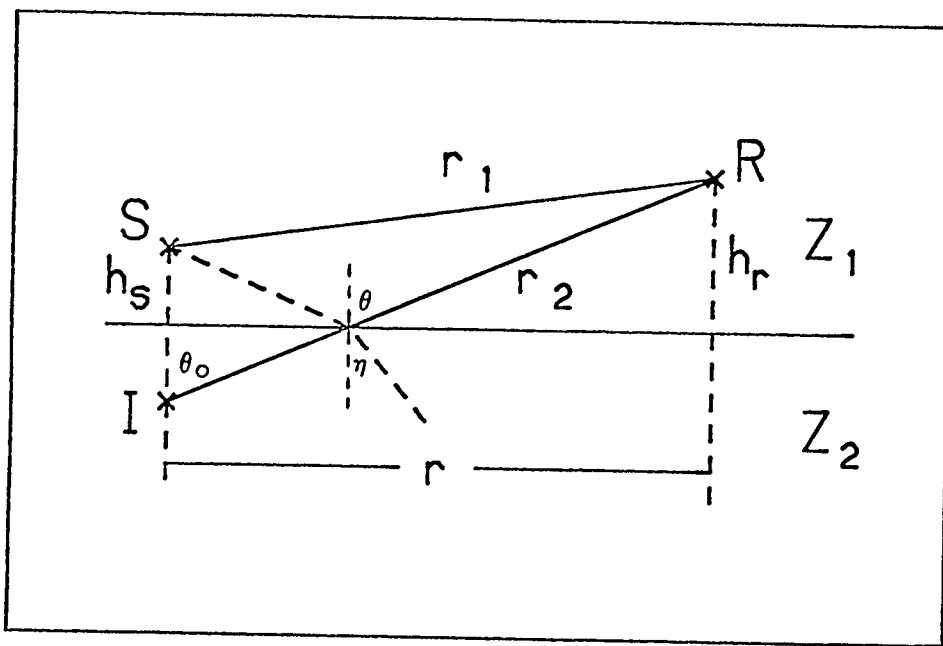


Figure 1.4.1. Source-receiver geometry for propagation of sound above a surface.

coefficient, R_p , is given by (Brekhevskikh, 1960)

$$R_p = \frac{\cos\theta - Z_1/Z_2(1 - k^2/k_2^2 \sin^2\theta)^{1/2}}{\cos\theta + Z_1/Z_2(1 - k^2/k_2^2 \sin^2\theta)^{1/2}} \quad 1.4.5$$

where $Z_1 = \rho c$ and Z_2 is the normal specific acoustic impedance of the ground. This is the reflection coefficient used by Rudnick (1947) in his early paper concerning the propagation of an acoustic wave along a boundary.

Both Z_2 and k_2 are, in general, complex quantities for the usual partially absorbing surface. Delany and Bazley (1970a) measured the acoustic properties of fibrous absorbent materials and showed that the characteristic impedance, Z_2 , and propagation coefficient, k_2 , could be given by a function of a single parameter, σ , the flow resistivity of the surface. For $Z_2 = R + iX$ and $k_2 = A + iB$ the relations are

$$\begin{aligned} R/\rho c &= 1 + 9.08(f/\sigma)^{-0.75} & X/\rho c &= 11.9(f/\sigma)^{-0.73} \\ A/(\omega/c) &= 1 + 10.8(f/\sigma)^{-0.70} & B/(\omega/c) &= 10.3(f/\sigma)^{-0.59} \end{aligned} \quad 1.4.6$$

Chessel (1977) extended the range of f/σ used by Delany and Bazley to show that most phenomena that have been observed and ground impedances that have been measured obey these power laws. Other models have been proposed including the four parameter model of Thomasson (1977) and the two

variable model of Rasmussen (1981) but the latter concludes that the simpler ground model of Delany and Bazley is a good approximation for most situations of interest.

Many solids are observed to be approximations of normally or locally reacting surfaces in which the transmitted wave is refracted in such a way that it propagates normal to the boundary between the two media. This occurs when the speed of sound in the lower medium is much smaller than in the upper, that is, $k_2 \gg k$. Piercy et al (1977) report that there is little evidence to show that the propagation of sound is not adequately predicted by this much simpler model for the ground surface. Chessel (1977) indicates maximum differences in sound levels using extended reaction models versus locally reacting surfaces of only 0.3 dB for source-receiver separations of up to 1000 m.

When the locally reacting model is used the boundary conditions (equations 1.4.2) reduce to one equation

$$-Z_2 \frac{\partial \Phi}{\partial z} = i\rho\omega\Phi \quad \text{or} \quad p/u_n = -Z_2 \quad 1.4.7$$

and the plane wave reflection coefficient becomes

$$R_p = \frac{\cos\theta - Z_1/Z_2}{\cos\theta + Z_1/Z_2} \quad 1.4.8$$

Equation 1.4.7 is remarkable in that any propagation in the ground that may or may not be present can be ignored. Only the sound pressure and normal component of the particle velocity in the air are required.

Now, consider the case of a point source above the plane surface. If this surface were perfectly flat, of infinite extent and perfectly reflecting, then the field at the receiver would be given by the sum of the fields of the source and its image I (Delany and Bazley, 1970b)

$$\Phi = \frac{e^{ikr_1}}{r_1} + \frac{e^{ikr_2}}{r_2} \quad 1.4.9$$

This method fails to give the correct solution if any of the three conditions above are not satisfied. Because of the different symmetries involved, spherical waves do not lend themselves to a straightforward fitting of the boundary conditions at a plane interface. Since the plane wave reflection coefficient is known it is natural to solve the problem by expressing the spherical waves in terms of an expansion of inhomogeneous plane waves
(Brekhovskikh, 1960):

$$\frac{e^{ikR}}{R} = \frac{ik}{2\pi} \int_C \int_{\phi=0}^{2\pi} \exp\{ik(x \sin\theta \cos\phi + y \sin\theta \sin\phi + z \cos\theta)\} \sin\theta d\theta d\phi \quad 1.4.10$$

where ϕ and θ are defined as in figure 1.4.2 and the path of integration for θ is shown in figure 1.4.3.

The integral over ϕ reduces to $2\pi J_0(kr \sin\theta)$ where J_0 is a zeroth order Bessel function, so that

$$\frac{e^{ikR}}{R} = ik \int_C J_0(kr \sin\theta) \exp(ikz \cos\theta) \sin\theta d\theta \quad 1.4.11$$

But $J_0(x) = \frac{1}{2} [H_0^{(1)}(x) + H_0^{(2)}(x)]$ where $H_0^{(1)}$ and $H_0^{(2)}$ are Hankel functions of the first and second kinds and $H_0^{(2)}(e^{-\pi i} x) = -H_0^{(1)}(x)$. Then it is easy to show that

$$\frac{e^{ikR}}{R} = \frac{ik}{2} \int_{C'} H_0^{(1)}(kr \sin\theta) e^{ikz \cos\theta} \sin\theta d\theta \quad 1.4.12$$

The total velocity potential at the receiver R will be given by the sum of the incident and reflected fields:

$$\Phi = \Phi_i + \Phi_r = \frac{e^{ikr_1}}{r_1} + \Phi_r \quad 1.4.13$$

Obviously

$$\Phi = \frac{e^{ikr_1}}{r_1} + \frac{ik}{2} \int_{C'} H_0^{(1)}(kr \sin\theta) R_p(\theta) e^{ik(h_r + h_s) \cos\theta} \sin\theta d\theta \quad 1.4.14$$

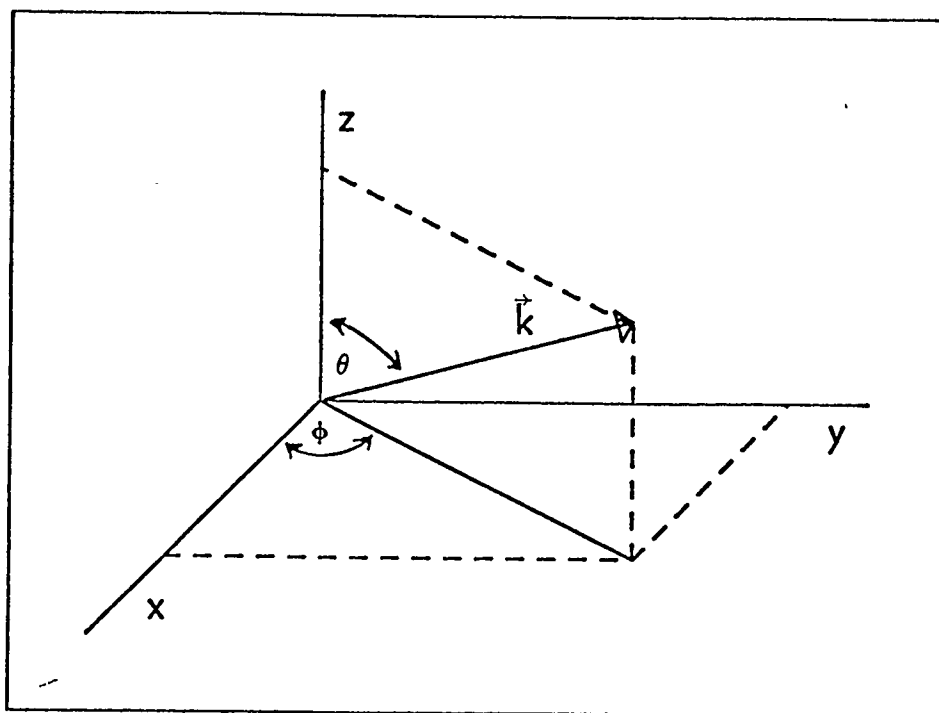


Figure 1.4.2. Angles of integration for equation 1.4.10.

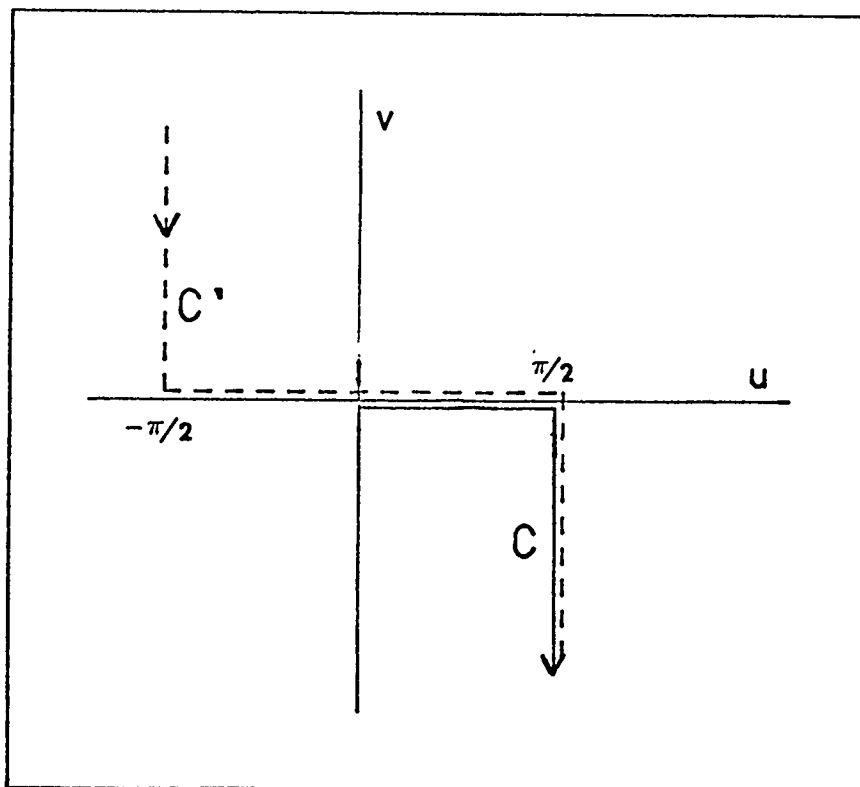


Figure 1.4.3. Contours of integration for $\theta = u + iv$ in equations 1.4.10 and 1.4.12.

This is the exact solution of the problem and is often written (Kawai et al, 1982)

$$\Phi = \frac{e^{ikr_1}}{r_1} + \frac{e^{ikr_2}}{r_2} + \Phi_L$$

1.4.15

$$\Phi_L = \frac{ik}{2} \int_C e^{ik(h_r + h_s)} \cos \theta H_o(1) (kr \sin \theta) \{R_p(\theta) - 1\} \sin \theta d\theta$$

Much of the theoretical literature is concerned with reducing equation 1.4.15 to forms that yield clearer interpretations of the radiated field. Wenzel (1974) suggests that a surface wave may be present for surfaces with a reactive component of impedance that is positive (representing a stiffness) and equal to or greater than a certain function of the resistive component. Such a wave propagates through the air in close proximity to the ground with an amplitude that decreases exponentially with height, and can lead to an amplification of the wave near the boundary. However, Embleton et al (1976a) claim that there are few measurements that indicate unambiguously the existence of surface waves over real surfaces outdoors.

Many papers deal with asymptotic solutions of equation 1.4.15 in the near- or farfields and in the cases of finite and high impedances (Thomasson, 1976; Kawai et

al, 1982; Chien and Soroka, 1975 and 1980; Donato, 1976). Attenborough et al (1980) compare many of these solutions showing that they are identical. While most make the assumption of the surface being locally reacting others are concerned with similar approximations for other surface types (Habault and Filippi, 1981; Delany and Bazley, 1970b; Thomasson, 1977).

The expressions adopted for comparison with the measured SPL values in this work were first developed by Rudnick (1947) for a porous medium and by Ingard (1951) and Lawhead and Rudnick (1951) for a locally reacting surface. Only the results are given here. The interested reader is referred to Chien and Soroka (1975 and 1980), or Kawai et al (1982) for a derivation.

For the field at R due to a point source at S (see figure 1.4.1)

$$\Phi = \frac{\exp(ikr_1)}{r_1} + \frac{\exp(ikr_2)}{r_2} \left\{ (1-R_p)F(w) + R_p \right\} \quad 1.4.16$$

where $F(w)$ is the boundary loss factor

$$F(w) = 1 + 2iw^{\frac{1}{2}} \exp(-w) \int_{-iw^{\frac{1}{2}}}^{\infty} \exp(-u^2) du \quad 1.4.17$$

and w is called the numerical distance

$$w = \frac{ikr_2}{2} \{ \cos\theta + (z_1/z_2) \}^2 \quad 1.4.18$$

For computational purposes the following asymptotic series are suitable for evaluation of $F(w)$:

$$F(w) = 1 + i \exp(-w) (\pi w)^{\frac{1}{2}} - 2 \exp(-w) \sum_{n=1}^{\infty} \frac{w^n}{(n-1)! (2n-1)} \quad \text{for } |w| \leq 10$$

$$F(w) = - \sum_{n=1}^{\infty} \frac{(2n)!}{2^n n! (2w)^n} \quad \text{for } |w| > 10$$

Equation 1.4.16 is the Weyl-van der Pohl equation originally developed for studies of electromagnetic wave propagation (Banos, 1966; Wait, 1970). The first term on the right is the direct wave whose amplitude decreases inversely as the distance. The second and third terms make up the sound-field reflected from the ground. The third term alone is that of a reflected plane wave. The second term compensates for the fact that R_p is independent of the angle of incidence whereas the sound-field is incident at different angles. This term vanishes for plane waves arriving at a single angle of incidence, perfectly reflecting surfaces for which $R_p = 1$, and for large values of the numeri-

cal distance corresponding to high frequencies, long source-receiver separations and smaller surface impedances.

According to Embleton (1982) the second term is called the ground wave, separating it from the direct and reflected waves. The surface wave is part of the complex function F that can be separated analytically for certain ground conditions.

Most outdoor sound sources are close to the ground so that R_p approaches -1 and r_1 and r_2 become nearly equal. As a result the first two terms of equation 1.4.16 cancel producing an acoustical shadow region near the ground. It is the ground wave that determines the sound-field inside this zone.

If the source and receiver are both significantly above the surface then there is interference due to the path differences of the direct and reflected waves and phase change upon reflection at the surface. Figure 1.4.4 shows these effects for various values of source and receiver heights and separations as well as flow resistivities. The excess attenuations plotted on the vertical scale are relative to that expected for a point source in a free field. A positive attenuation indicates a lower SPL than expected for spherical spreading alone; a negative value indicates an enhancement of the field.

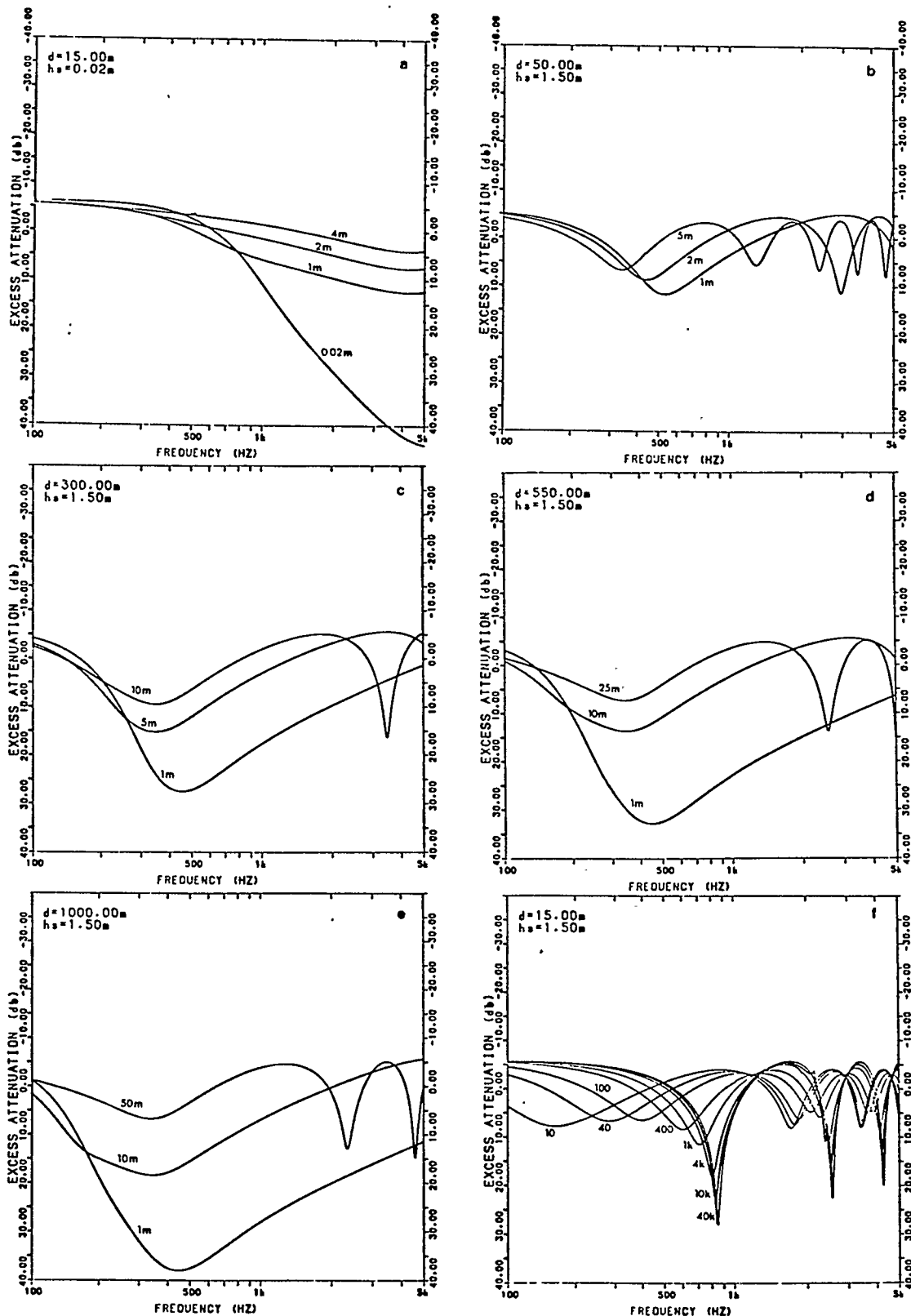


Figure 1.4.4. Theoretical excess attenuations for various source-receiver separations and heights and flow resistivities (d = source-receiver separation, h_s = source height): a-e) labels refer to receiver height (m), f) labels refer to the flow resistivity (cgs rayls).

1.5 Meteorological Effects

Inhomogeneities in the atmosphere have a profound influence on acoustic wave propagation. Temperature and wind gradients, and on a smaller scale turbulence, have quite different effects but both are manifestations of the same physical process, namely changes in the index of refraction along the propagation path.

A computer program developed by Jones and Stephenson (1975) and Georges (1971) has been employed to calculate three-dimensional acoustic-gravity ray paths in the atmosphere. The ray paths are calculated by numerical integration of Hamilton's canonical equations (Georges, 1971). This program can simulate three-dimensional wind and temperature profiles using model atmosphere subroutines by Georges (1971) or, using new routines developed in the course of this work, can incorporate real meteorological data acquired by tethersonde or other means. In the latter case wind, temperature and height information is entered into the program by a separate file and cubic spline interpolation (Burden et al, 1981) is used to model continuous wind and temperature profiles between data points.

Ray tracing also permits calculation of the excess attenuation of sound as a function of distance from the source by calculating the acoustic energy normally incident on a unit area a given distance from the source and comparing it to

that expected for spherical spreading alone. If ψ is the elevation angle of the emitted acoustic ray and assuming no change in the lateral spreading of the sound then the excess attenuation, EA, is given by

$$EA = -10\log_{10} \left| \frac{r}{\sin\psi} \frac{d\psi}{dr} \right| \quad 1.5.1$$

where r is the distance from the source. Reflections from the surface have been ignored and where more than one ray is incident at the receiver intensities from each have been added. When $\frac{dr}{d\psi} = 0$ equation 1.5.1 predicts infinite sound levels and a more complete solution is needed.

The presence of temperature or wind gradients or a combination of both can lead to regions of enhanced sound levels or shadow zones, areas where the sound pressures are reduced as indicated in figure 1.5.1. These shadow regions, it should be pointed out, are unrelated to the shadow zones created by the ground effect discussed in the previous section.

Wind gradients are almost always present in the boundary layer of the atmosphere because of viscous drag on the air at the ground surface. If a simple positive linear velocity gradient is assumed, then for propagation upwind the speed of sound will decrease with height and the ray paths will describe circular arcs directed upward. For down-

wind propagation the rays are directed downwards as in figure 1.5.1a. Note that the steps apparent in the ray paths are an artifact of the ray tracing program and have no physical significance.

On warm, sunny days solar heating of the earth's surface leads to temperature lapse conditions, or a negative temperature gradient. Again, assuming a linear gradient, equation 1.2.2 indicates that the sound velocity decreases with height and the ray paths will once more be circular arcs directed upwards (figure 1.5.1b). The situation is often reversed during calm, clear evenings when radiative cooling of the ground results in a temperature inversion, an increase in temperature with height. Now the sound rays are directed downwards as illustrated in figure 1.5.1c.

It can be seen that downwind sound propagation and temperature inversions can enhance sound levels at the surface. Often this effect is large enough to negate the effect of the ground on sound propagation (Foss, 1979; Wiener and Keast, 1959). The effects of temperature inversions are usually apparent only for distances greater than 500 m (Embleton, 1982). A more detailed account of their effect will be given in chapter four. According to Piercy et al (1977) excess attenuations can be approximately 0 dB

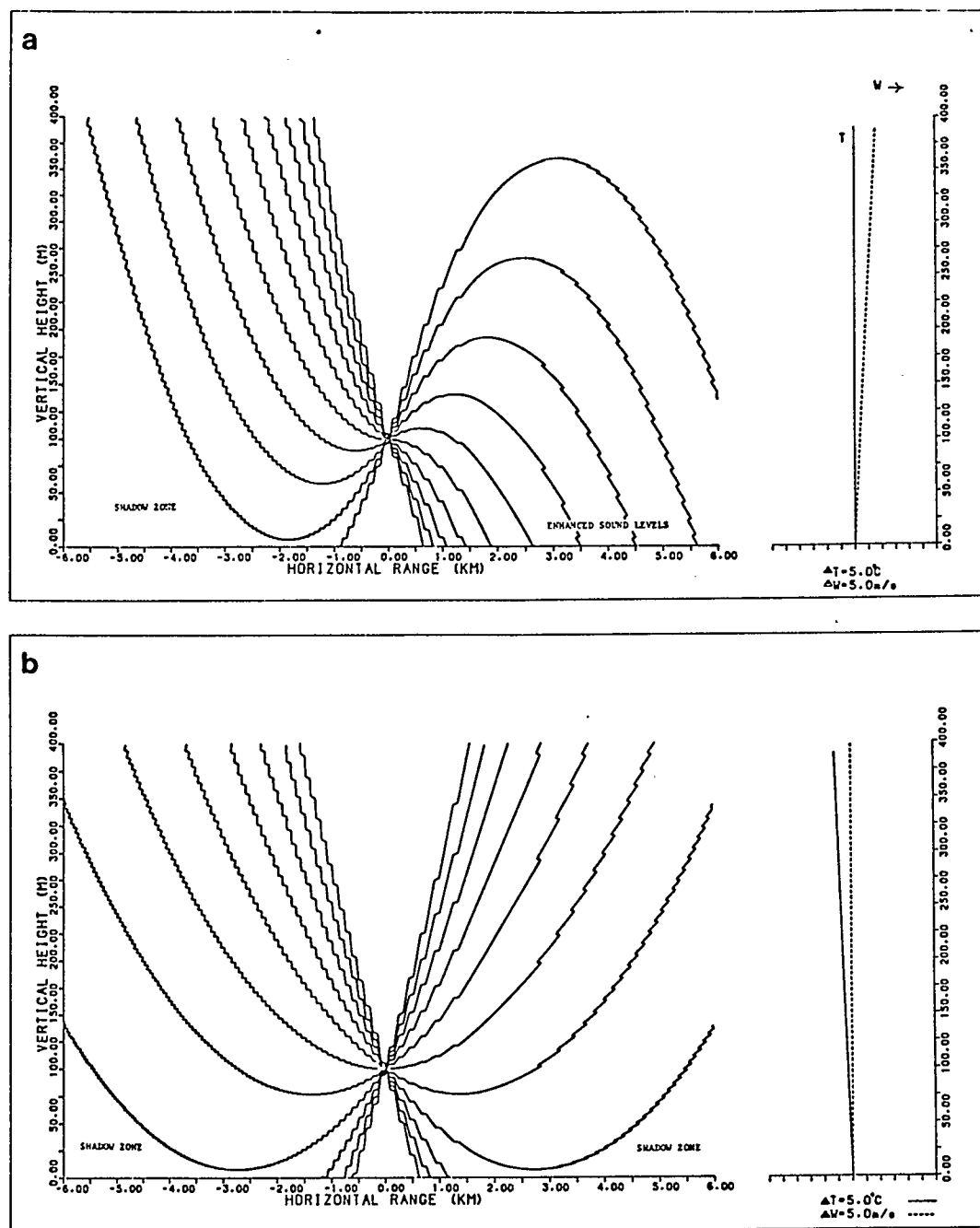


Figure 1.5.1. Ray paths for different meteorological conditions:

- constant wind gradient from the surface
- temperature lapse

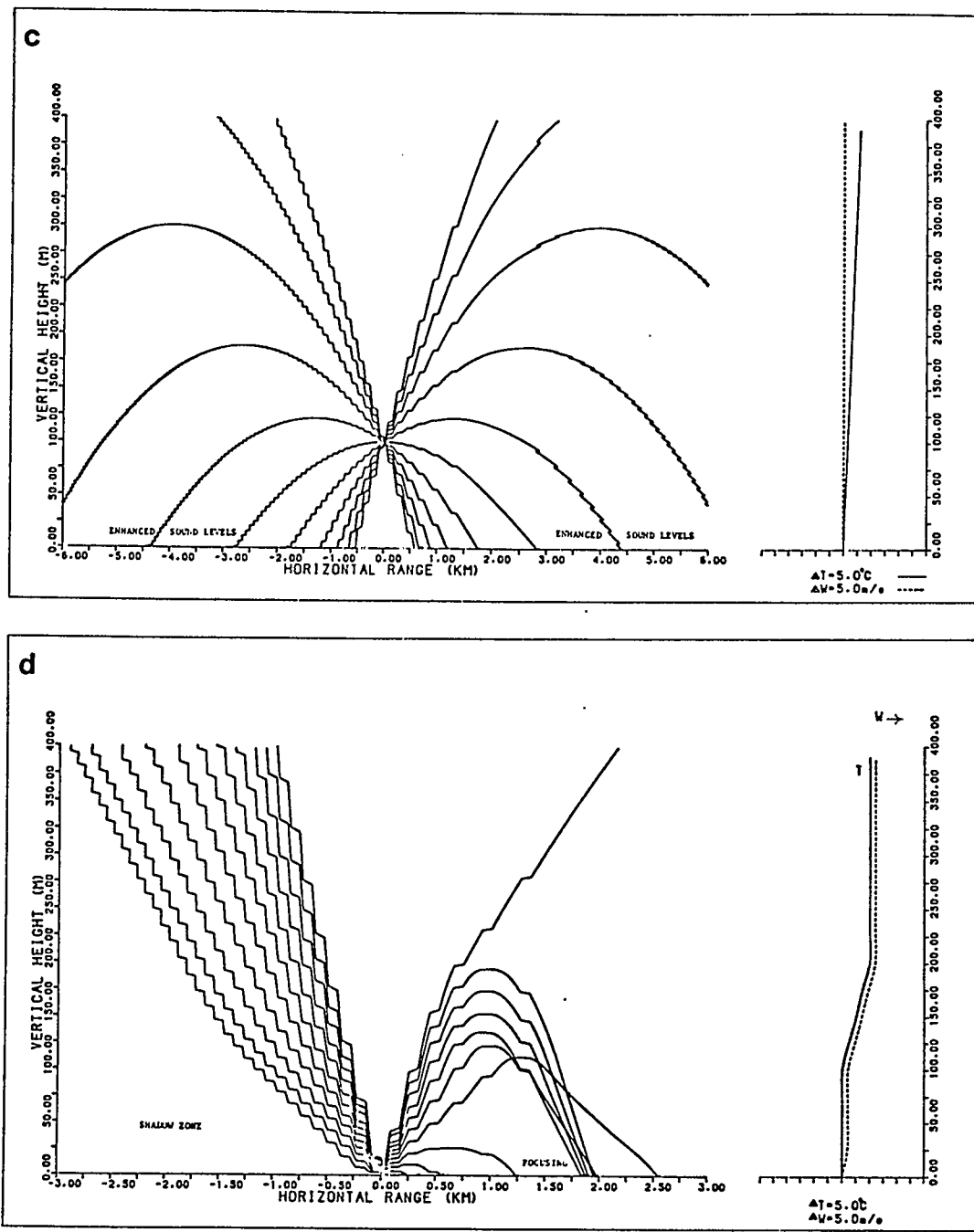


Figure 1.5.1. continued...

- c) Ground-based temperature inversion
- d) Elevated temperature and wind gradients.

in conditions of downward refraction and 20 dB during conditions of upward refraction.

Figures 1.5.1a, b and c display the effect of ground-based wind and temperature gradients. In the case of elevated temperature inversions or wind shear the same refraction of sound can lead to focusing effects. Sound rays projected at different angles from a source may return to the surface in the same vicinity creating SPL's much higher than expected if geometric spreading were the only process acting. For various combinations of wind and temperature gradients these caustics may appear as close as one kilometer from the source. Figure 1.5.1d shows the situation for elevated wind and temperature gradients of 10 m/s/100 m and 10°C/100 m from 100 m to 200 m above the surface. Focusing occurs at the surface approximately 1900 m downwind from the source. This phenomenon, which occurs routinely during the onset of the Southern Alberta Chinook during which elevated inversions strengths as large as 40°C/100 m are recorded, is investigated in chapter four.

Turbulence is created when large eddies are formed in the atmosphere because of instabilities in the boundary layer near the ground. Turbulence of various scales is present at all times, the intensity being high during lapse conditions and low during stable inversions. Temperature fluctuations of 5°C and root-mean-square fluctuations of wind

speed of about one-third of the mean wind speed are common (Embleton, 1982).

These fluctuations lead to local fluctuations in the index of refraction of the air which in turn lead to fluctuations in the amplitudes and phases of sound waves. The effects are two-fold. Firstly, the turbulence causes some scattering of the sound wave. For upward refracting conditions (figures 1.5.1 a and b) no sound is expected in the shadow zone. In fact, the excess attenuation is usually limited to between 10 and 30 dB because of the turbulent scattering of the acoustic waves (Embleton, 1982). Secondly, since both the phase and amplitudes of the sound waves are fluctuating the interference effects discussed in section 1.4 tend to be less pronounced. The direct and reflected waves are now only partially coherent at best since they travel through different portions of an inhomogeneous atmosphere.

Daigle et al (1978) and Daigle (1979) have developed a theory that gives excellent agreement with experimental SPL's. Expanding on work by Ingard and Maling (1963) and

Chessel (1977) they start with equation 1.4.16 and show that the time averaged mean-square sound pressure is

$$\langle \bar{p}^2 \rangle = \frac{2}{r_1 r_2} \left[\frac{\langle a^2 \rangle}{2} \left(\frac{r_2}{r_1} + |Q|^2 \frac{r_1}{r_2} \right) + \frac{r_2}{2r_1} \left(1 - |Q| \frac{r_1}{r_2} \right)^2 \right. \\ \left. + |Q| + |Q|(1 + \langle a^2 \rangle \rho_a) \cos(\phi + \zeta) \exp\{-\sigma_1^2 (1 - \rho_\delta)\} \right] \quad 1.5.2$$

where

$$\phi = k(r_2 - r_1) \quad Q = R_p + (1 - R_p)F = |Q|e^{i\zeta} \quad 1.5.3$$

and R_p and F are defined in equations 1.4.5 and 1.4.17, while $\langle a^2 \rangle^{1/2}$ is the standard deviation of the amplitude fluctuations, ρ_a and ρ_δ the amplitude and phase covariances respectively, and σ_1 is the standard deviation of the wave number fluctuations, all of which can be determined from observations of various meteorological parameters such as fluctuations in temperature and wind (see appendix A).

Figure 1.5.2 shows some of their results for distances up to 1100 meters.

A recent paper (Clifford and Lataitis, 1983) gives a more rigorous mathematical treatment but the results differ only slightly giving no better agreement than that obtained by Daigle et al according to the authors.

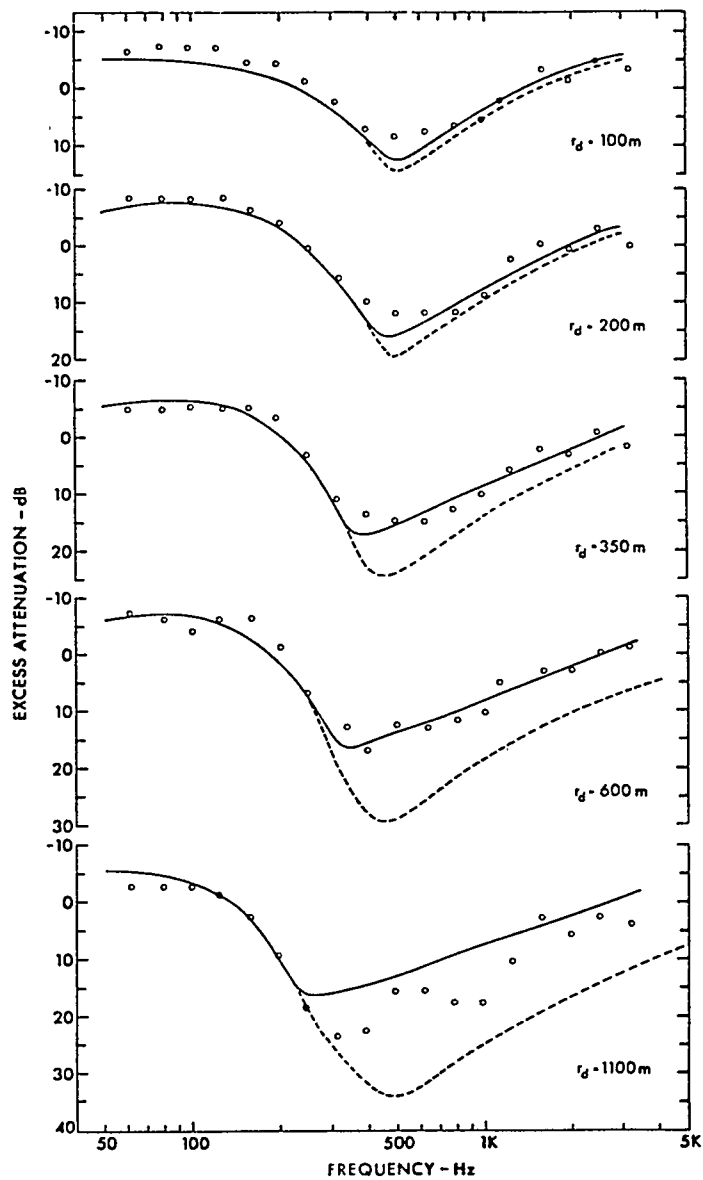


Figure 1.5.2. Comparison of measured sound levels (o) (Parkin and Scholes, 1964) with values predicted by coherent acoustic theory --- (equation 1.4.16); turbulent theory — (equation 1.5.2) with $\langle \mu \rangle^2 = 2.0 \times 10^{-6}$, $\rho_a = \rho_\delta = 0.80$, $h_s = 1.8\text{m}$, $h_r = 1.5\text{m}$, $\sigma = 300$ cgs rayls (from Daigle, 1979).

CHAPTER II

EXPERIMENTAL EQUIPMENT AND PROCEDURE

2.1 Overview of Equipment

The instrumentation for the investigation of sound propagation under temperature inversion conditions was designed and built by the Lower Atmospheric Physics and Acoustics Group at the University of Calgary. The equipment consisted of a sound source, four microphones with built-in preamplifiers and a receiver. Raw data was recorded on magnetic tape for later reduction. Provision was also made for the use of a chart recorder for immediate monitoring of the data. Figure 2.1.1 shows a schematic of the instrumentation. A more detailed description of each component follows.

2.2 Receiver

Four microphones, General Radio type 1560-9065, were placed in the field and connected to the receiver by cables up to one kilometer in length. Each was mounted on a tripod stand with height above the surface adjustable from 0.20 m to 2.0 m.

The output from each microphone is amplified 40 dB by a FET-input preamplifier which is part of the microphone

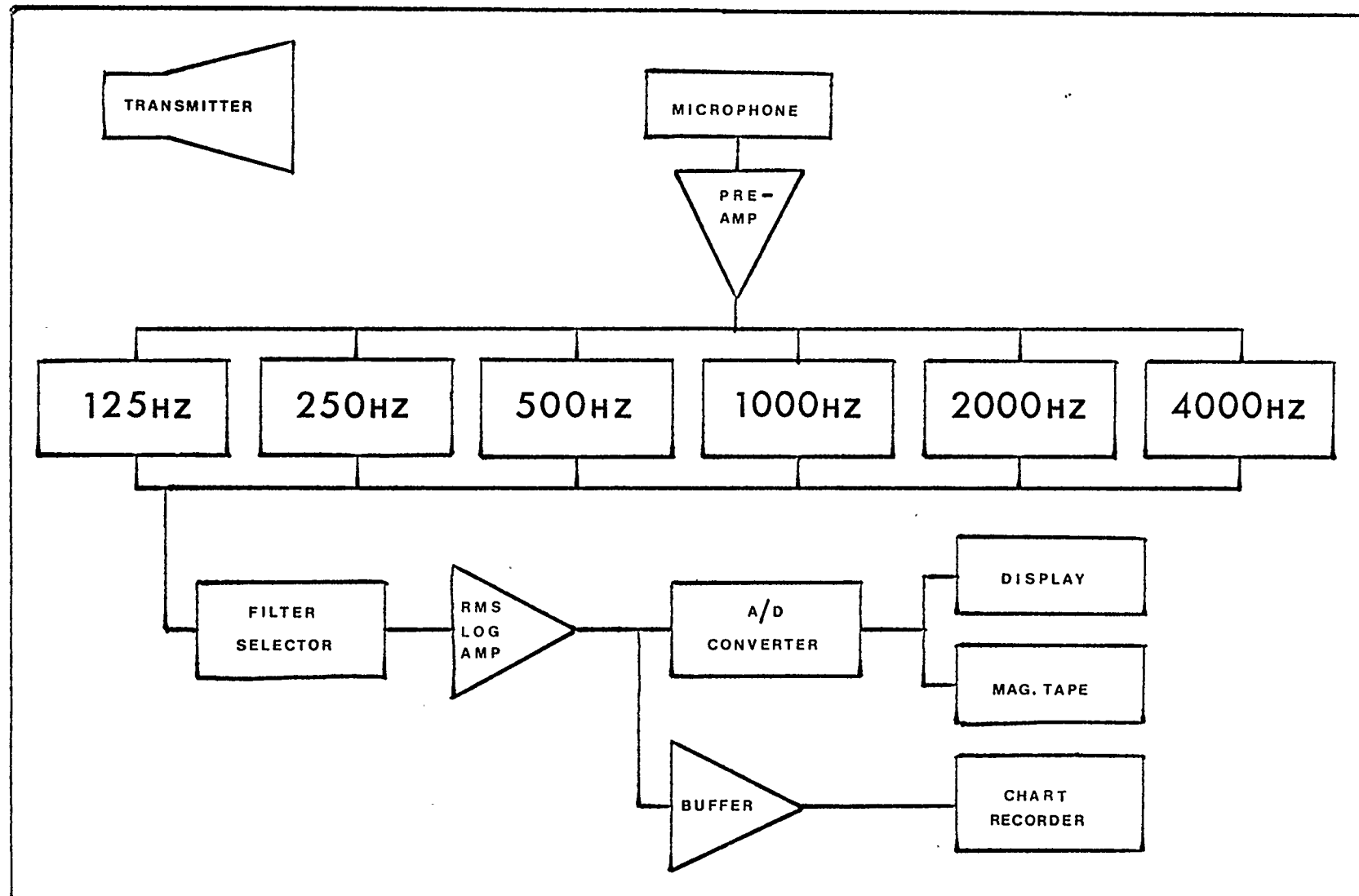


Figure 2.1.1. Schematic of electronics, one channel only.

assembly. A low impedance line driver drives the length of the cable between the preamplifier and the receiver reducing stray noise pick-up.

The receiver sees the microphone outputs as four separate channels. Each signal is sent through one of six octave band-pass filters per channel with Q's of 10 and gains of 14 dB. The output of the filters, which range from 125 Hz to 4000 Hz, is controlled by the selector relays which are in turn controlled by the telemetry channel. The transmitter sends a digitally encoded frequency identifier which is received by the first channel and converted to a control pulse for all four channels. Each channel then selects the same filter.

The filter stage is followed by gain and attenuation switches that control the gain of the system from -60 dB to +60 dB in 20 dB increments. The higher levels are required for low amplitude signals while the lower settings are primarily used for calibration of the equipment although the channel nearest the sound source may require an attenuation of -20 dB to bring the signal within the receiver's dynamic range.

The receiver's RMS logarithmic amplifier has a dynamic range of about 65 dB over which it is linear to within 1/4 dB. The lower limit of its sensitivity is governed by thermal and electronic noise and is on the

order of 20 dB. Saturation of the preamplifier occurs for signals of 130 dB or greater.

The analog output of the logarithmic amplifier is converted to eight bit binary data by means of an A/D converter, the accuracy being limited to the least significant bit. Data resolution has proven to be about 3.8 bits/dB or 0.26 dB/bit.

A Zilog Z-80 microprocessor and its associated hardware controls the A/D conversion rate as well as the data transfer to the 9-track Pertec tape drive. Four hundred and eighty samples were taken per channel, one every ten milliseconds. For propagation distances greater than 550 m appropriate time delays for each channel were implemented so that the same portion of the waveform was sampled at each microphone location. For a 1000 m separation of channels A and D this delay amounted to about 3.0 seconds. Data transfer to the magnetic tape was at 800 bits per inch (bpi) and included the digital data as well as frequency information, elapsed time, appropriate headers for calibration and data records and the number of samples taken.

A backup system consisted of a Honeywell 12 channel high speed galvanometer chart recorder. The volume of paper generated (six inches per second or more) minimized

the usefulness of this system and indeed, dictated the conversion to digital.

2.3 Transmitter

For short-range sound propagation the transmitter consisted of an 8085 microprocessor-controlled sine wave burst generator, a three hundred watt power amplifier and an Altec Lansing compression driver (model 290-8k) coupled to an exponential horn 0.61 m long and with an open diameter of 0.10 m.

The transmitting sequence begins with the computer sending out a 125 Hz frequency identifier via telemetry centered on a 9 kHz carrier frequency. One-half second later the generator produces a short 125 Hz burst. This delay not only gives the relay contacts time to dampen and the RMS circuit time to settle but also provides ample time to transfer the data acquired during the previous cycle to the magnetic tape. Then, another delay of several seconds occurs during which time the data acquisition takes place. The cycle repeats for the other five frequencies and then begins again at 125 Hz.

The frequency-bursts and the associated delays are software-controllable. For the short-range studies a burst duration of 1/10 second was employed and the burst generator cycled through the six frequencies in

approximately thirty seconds. At this rate it was possible to gather twelve hours of continuous data on a single tape.

Unfortunately the power amplifier and loudspeaker assembly provided an insufficient sound level for distances much greater than 500 m. Even at this range because of the inefficiency of the driver at low frequencies only the upper four frequencies were consistently above the background noise level. For long-range sound propagation atmospheric absorption severely attenuates signals above 500 Hz. Losses of 35 dB are typical at 2000 Hz for source-receiver distances of 1500 m. For these distances a source of low frequency noise (125 Hz to 500 Hz) for which absorption is much less important was required. The use of two propane-powered cannon was decided upon after much experimentation. These were capable of producing extremely short bursts with SPL's of approximately 100 dB at 125 Hz and 250 Hz at a distance of 130m. Levels decreased to between 80 and 90 dB at 4000 Hz. Repetition rates were approximately one to one and one-half minutes for each cannon. With periodic maintenance these sources operated continuously for more than two weeks with a 100 lb propane tank.

The transmitter for long-range studies consisted of the cannon and the burst generator, still required for control of telemetry. A minor software change lengthened the time delay between each cycle to accommodate the longer

propagation times. A single tape could now hold more than twenty-four hours of data.

2.4 Calibration

Initially the electronics was calibrated before and after each data run to check the linearity of the system and to establish a means of converting the binary data to actual decibel readings. At no time did a nonlinearity of the equipment manifest itself. In fact, the excellent stability of the system soon made it apparent that the end-of-run calibration was unnecessary and it was discontinued.

In calibrating the instrument a General Radio pistonphone, model 1562-A, is set to its 1000 Hz range and placed over one of the microphones. This provides a standard sound source of 114 dB (relative to 2×10^{-5} N/m²). The receiver is set to the calibrate mode and the 1000 Hz filter is selected manually. The signal's binary display value is recorded for the 0 dB, -20 dB, -40 dB and -60 dB settings of the attenuation switch. These values can be plotted on a calibration graph for an on the spot check of the behaviour of the instrument. The information is also written on the magnetic tape where processing will allow for the determination of the minimum sound level recorded, resolution and the dynamic range. On

the 0 dB gain setting typical values are 45.0 ± 0.6 dB, 3.8 ± 0.1 bits/dB and 67.6 ± 1.3 dB respectively. The same procedure is then used on the remaining three channels.

2.5 Data Reduction

At the end of the data acquisition information on the magnetic tape was processed on the Honeywell Multics computer of the University of Calgary's Department of Academic Computing Services.

Routines have been written which allow for various length time averages of SPL's subject to minimum SNR criteria to be calculated and printed. Plots of the acoustic waveform at each channel can be generated for either individual records or for the above averages. The background noise level is determined for each channel and is printed along with the signal strengths, although for some channels this level represents the minimum recorded noise level rather than the actual background noise level.

Various plotting subroutines allow for graphical representations of the SPL's as functions of time, distance and frequency, both measured and theoretical.

In instances where the burst generator triggered loudspeaker was employed five minute time averages were chosen as a compromise to minimize both printout which shorter averages would give and loss of information longer averages

would entail. When the cannon was the source the inherent randomness of its backfiring necessitated examining each record individually for a satisfactory signal. An S/S+N ratio of 30 dB was required at the microphone 130 m from the source in order to receive a useful signal at the furthest channel. Since each successive burst provided a different sound level averaging of the signals was only valid after each had been normalized to a single level at the channel nearest to the source.

2.6 Experimental Procedure

Investigations of temperature inversions and their effect on sound propagation were conducted at Springbank Airport located 20 kilometers west of Calgary and at the farm of David Irwin near Vulcan, Alberta approximately 100 kilometers south of Calgary. At Springbank the Department of Physics of the University of Calgary has operated Doppler and monostatic SODAR from a trailer on land leased by the airport since 1980. The field used is very flat for about one kilometer with a rise of about fifteen meters in the easternmost half kilometer. The area of interest for short-range propagation had been plowed repeatedly during the summer and fall prior to the data acquisition while the hillier terrain was grassland.

The experimental apparatus was deployed at the two sites in two different manners for the investigations of the nocturnal inversion. First, the effects, if any, that an inversion has on short-range propagation of sound were studied. At the Springbank site four microphones were placed at distances of 10, 50, 300 and 550 meters from the loud speaker generating pure tones and the ensuing sound levels were recorded. At the Vulcan site, the microphones were located on a longer baseline with source to receiver distances of 130, 830, 1730 and 2180 meters and the propane cannon was used as the sound source. In both cases the microphone closest to the sound source was used as a reference for determining excess attenuations at the other receiver locations.

Data runs in each study were virtually identical. Each microphone was calibrated and checked for linearity. A portable monostatic SODAR was in operation during each run to allow for continuous monitoring of the inversion layer height and extent. At Vulcan, a tethersonde enabled both temperature and wind profiles to be obtained to heights of several hundred meters. At Springbank, hourly values of ground temperature and wind were recorded as well as the relative humidity.

The excess attenuations measured at the second microphone locations during the investigations permitted the deter-

mination of values for the flow resistivity, σ , and hence the ground impedance as will be discussed in the next chapter.

The experimental apparatus for investigating the focusing phenomena of elevated temperature inversions was identical to that used for the study of the long-range effects of the ground-based inversions. In fact, it was the presence of strong westerly winds associated with the southern Alberta Chinook that suggested the east-west placement of the source and receiver; theoretical calculations show that the most noticeable focusing will appear downwind from the source.

CHAPTER III

GROUND IMPEDANCE

3.1 Review

In order to calculate sound intensities near a surface using equations 1.5.2 and 1.5.3 the plane wave reflection coefficient given by equation 1.4.5 must first be determined. This in turn requires a knowledge of the normal acoustic impedance or ground impedance, z_2 , of the surface involved, either through a measurement of the flow resistivity, σ , and use of Delany and Bazley's model (equation 1.4.6) or by direct measurement of the real and imaginary components of $z_2 = R + iX$.

Before proceeding with the description of the experimental technique used for determining z_2 and the analysis of the results it may prove useful to outline a few of the methods currently employed to measure z_2 or σ . These entail acoustical methods using the physics already described or direct analysis of the surface itself with specially designed apparatus.

Two theoretically simple methods enable one to obtain an estimate of the magnitude of the ground impedance, $|z_2|$. The first of these assumes both source and receiver are on

the impedance surface in which case $\cos\theta$ is small compared to z_1/z_2 and R_p in equation 1.4.5 approaches -1.

Ignoring turbulence the sound field, equation 1.4.16, then becomes

$$\Phi = 2F \frac{\exp(ikr_2)}{r_2} \quad 3.1.1$$

Defining the cutoff frequency, v_c , as the frequency at which the field in equation 3.1.1 has fallen 3 dB below that expected from the inverse square law alone, Embleton et al (1976a), using equation 1.4.18 and 3.1.1 and results of Wait (1970), demonstrate that

$$\frac{2\pi v_c}{c} |z_1/z_2|^2 \approx 4 \quad 3.1.2$$

from which an estimate of $|z_2|$ can be obtained.

In the second case only the source is on the ground. Far above the cutoff frequency with $w \gg 0$ and $F \approx 0$ equations 1.4.16 and 1.4.8 give

$$|\Phi| = \frac{2 \cos\theta}{|r| |z_1/z_2|} \quad 3.1.3$$

Hence, by observing the excess attenuations inside the shadow zone one can again determine $|z_2|$.

Two other methods take advantage of the interference effects of the direct and reflected acoustic waves to

measure Z_2 . With an inclined track the microphone is moved along the reflected ray path shown in figure 1.4.1. Given an accurate determination of the geometry of the system one can calculate the real and imaginary components of Z_2 by measuring the changing interference pattern at a given frequency.

The concept behind the impedance tube is similar only here the acoustic wave is normally incident upon the surface. By observing the maxima and minima of the standing wave pattern created by a sound source in the tube the components of Z_2 can once again be deduced (Talaske, 1980).

Some experimentalists have made direct measurements of the flow resistivity of various surfaces. Bolen and Bass (1981) measured the rate of air flow through a cylindrical sample of earth as a function of the differential pressure across the sample. The flow resistivity is the observed ratio of the pressure drop to the volume current. Equation 1.4.6 then gives $Z_2 = R + iX$. Delany and Bazley (1970a) used this type of measurement of the flow resistivity, impedance tube measurements of the acoustical impedance of the same fibrous, absorbent materials and regression analysis to obtain the power law relations given in equations 1.4.6.

Figure 3.1.1 shows measurements of the ground impedance for grass covered land reported by Piercy et

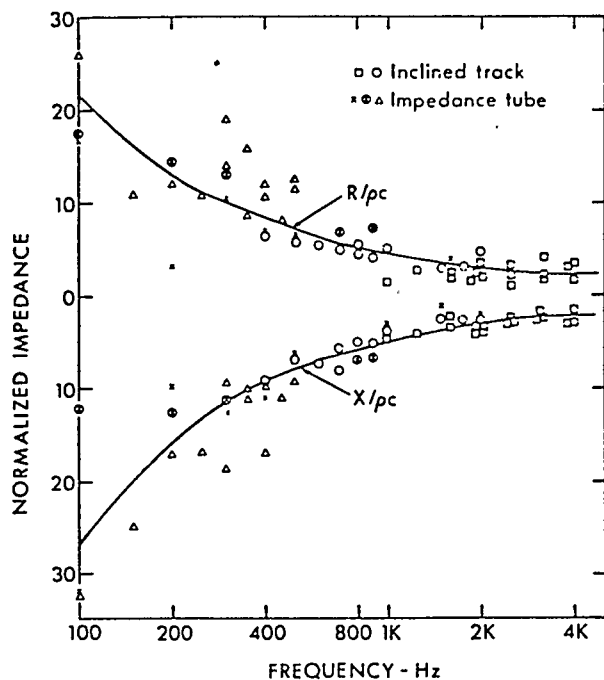


Figure 3.1.1. Experimental values of the normalized specific normal impedance of grass-covered ground (Daigle et al, 1983).

Description of Surface	Flow Resistivity in rayls (CGS units)
Dry snow, new fallen 10 cm deep	15 to 30
Sugar snow	25 to 50
In forest, pine or hemlock	20 to 80
Grass: rough pasture, airport, public buildings, etc.	150 to 300
Roadside dirt, ill-defined, small rocks up to 10 cm diameter	300 to 800
Sandy silt, hard packed by vehicles	800 to 2500
"Clean" limestone chips, thick layer (12.7 to 25.4 mm mesh)	1500 to 4000
Old dirt roadway, fine stones (6.35 mm mesh) interstices filled	2000 to 4000
Earth, exposed and rain-packed	4000 to 8000
Quarry dust, fine, very hard-packed by vehicles	5000 to 20,000
Asphalt, sealed by dust and use	> 20,000

*Values give best fit between measured sound spectrum and that predicted by a one-parameter model

Table 3.1.1. Flow resistivities of various ground surfaces (Embleton, 1982).

al (1977). The curves represent the best fit given by the Delany and Bazley model. The plot clearly indicates that the ground impedance increases at low frequencies. This is consistent with the propagation of sound in porous materials. When sound impinges on the surface air is forced into the pores alternately compressing the air in them and encountering resistance in the walls and surrounding material. The velocity in the pores is slower than in the air above the surface and is highly frequency dependent. The amount of sound reflected will depend on how much energy is absorbed by the ground and by the phase changes that occur in the surface. When all the pores are not of the same depth different path lengths will give rise to phase cancellations, the effect being most noticeable for higher frequencies.

Table 3.1.1 contains ranges of the flow resistivity measured for various surface types.

3.2 Field Measurements of Ground Impedance

The technique decided upon in this work to obtain values for the ground impedance of various surfaces relies on a phenomenon observed by several workers (Foss, 1979; de Jong et al, 1982). As figure 1.4.4f demonstrates, the attenuation of sound at low frequencies is strongly dependent on the flow resistivity and at high frequencies

is much less dependent of the nature of the surface. Meteorological conditions on the other hand influence attenuations at high frequencies more than at low frequencies. Thus it is possible to obtain an estimate of the flow resistivity and hence the ground impedance by making a best fit of theoretical excess attenuations below a certain critical frequency to values obtained in the field with the flow resistivity, σ , as an adjustable parameter.

The procedure consisted of minimizing

$$E(\sigma) = \sum_{i=1}^3 (|EA_m(f_i)| - |EA_c(\sigma, f_i)|)^2 \quad 3.2.1$$

where $EA_m(f_i)$ are the measured excess attenuations at 125, 250 and 500 Hz and $EA_c(\sigma, f_i)$ are the excess attenuations calculated using equations 1.5.2 and 1.5.3. The fit to the field measurements was improved further by adjusting the fluctuating index of refraction parameter $\langle \mu^2 \rangle$ (see appendix A). Altering the values of $\rho_a = \rho_\delta$ and L in equation 1.5.2 from the values of 0.80 and 1.1 m adopted by Daigle et al (1978) did not lead to an improved fit of theory to experimental data. These parameters were therefore treated as constants.

This type of procedure has been employed by Habault (1981) along with a similar technique treating the source to receiver distance as the adjustable parameter.

Since the focus of this work was concerned with gathering information concerning sound enhancements resulting from temperature inversions the former method was found to be most suitable as ground impedance information could be extracted without disrupting the deployment of the experimental apparatus for inversion investigations.

3.3 Experimental Results

Figure 3.3.1 shows the experimental results. The flow resistivities of three types of surfaces were determined. Figure 3.3.1a is for the plowed field at Springbank Airport. The best fit curve gives a flow resistivity of 60 cgs rayls, consistent with a soft, very porous surface.

Figure 3.3.1b is for the same field but with a layer of fresh snow about 10 cm deep. A very good fit to the data is obtained with a flow resistivity of 30 cgs rayls.

Finally, figure 3.3.1c indicates a flow resistivity of 170 cgs rayls for the grass field at the Vulcan site. Since continuous meteorological information was not available there the data has been averaged for several sunny afternoons. This removed much of the effect of variable wind speeds and directions on the excess attenuations. In any case the fit to the data is almost exact. The standard deviations of the excess attenuations at each frequency have been plotted as error bars to indicate the

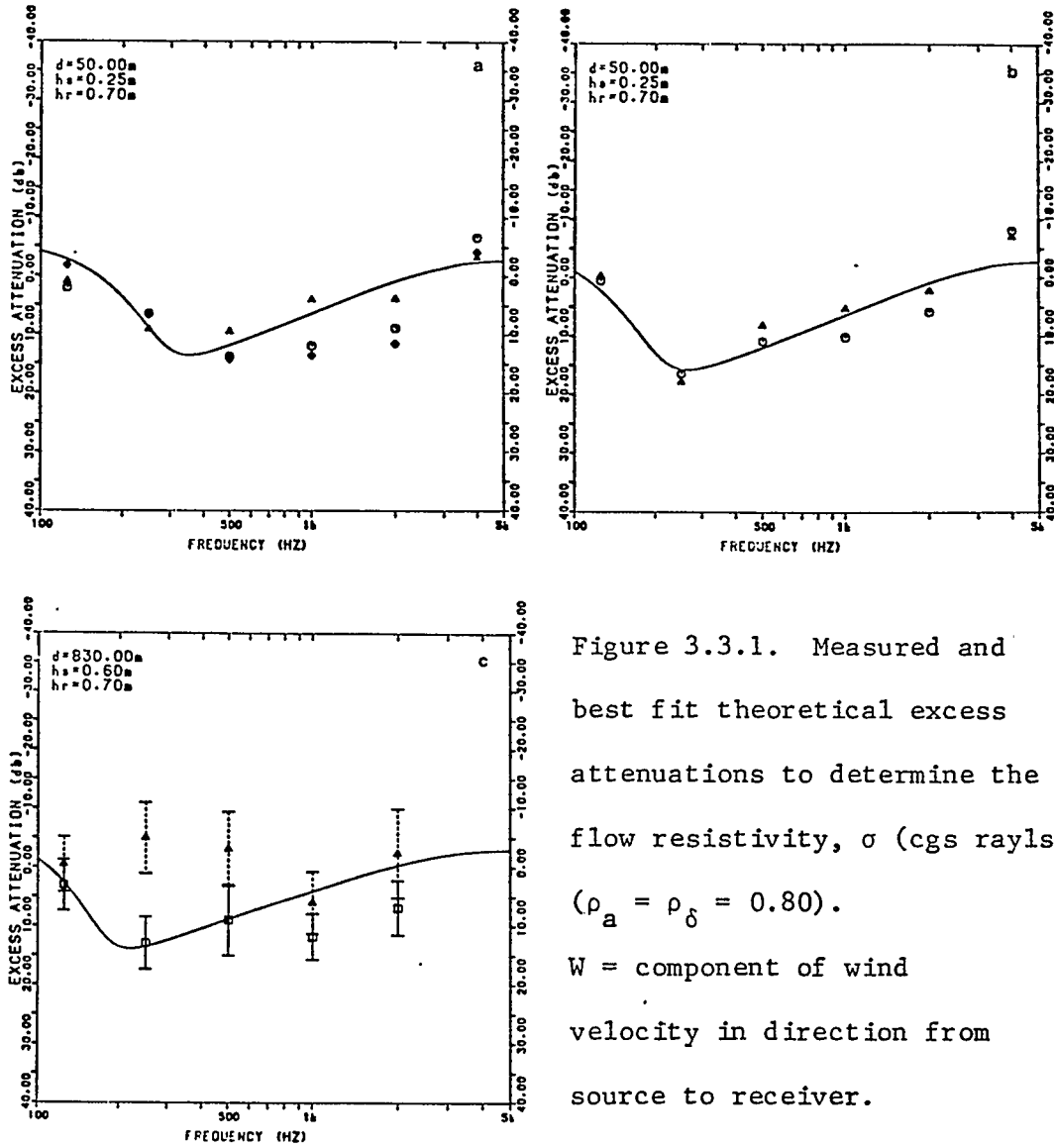


Figure 3.3.1. Measured and best fit theoretical excess attenuations to determine the flow resistivity, σ (cgs rayls) ($\rho_a = \rho_\delta = 0.80$).
 W = component of wind velocity in direction from source to receiver.

a) plowed field at Springbank Airport: $\sigma=60$, $\langle \mu^2 \rangle=2 \times 10^{-5}$,

\diamond : $W=1.0$ m/s, Δ : $W=0.2$ m/s, \circ : $W=-2.0$ m/s.

b) snow-covered field at Springbank: $\sigma=30$, $\langle \mu^2 \rangle=2 \times 10^{-5}$,

Δ : $W=0.0$ m/s, \circ : $W=-0.4$ m/s.

c) grass-covered field at Vulcan site: $\sigma=170$, $\langle \mu^2 \rangle=3 \times 10^{-6}$,

\square : temperature lapse data, Δ : nocturnal inversion data.

range of the measurements. Atmospheric absorption is so large at 4000 Hz that data at this frequency have not been included. It should also be noted that 830 meters from the sound source is perhaps a rather extreme distance for determining the flow resistivity by this best fit method. While a small temperature lapse seemed to have little effect on the excess attenuation at 500 Hz and below it will be seen in chapter four that the same cannot be said for a strong ground-based or elevated inversion.

Figures 3.3.1a and b also indicate the effect of wind gradients on the measured excess attenuations. Data was obtained late in the evening and in the early morning before sunrise while there was a ground inversion present. A breeze from receiver to source (denoted by a negative velocity) negated any effect of the ground inversion and increased the attenuation while a wind from source to microphone caused a slight enhancement of the sound level. Notice however, that the effect on the frequencies of 500 Hz or lower was very small, strengthening this method of measuring the flow resistivity.

In figure 3.3.1c any bias of excess attenuation caused by various wind conditions has been removed but the temperature lapse present during the sunny afternoons led to an appreciable increase of about 10 dB in the excess attenuations at 1000 and 2000 Hz.

In summary, the measured flow resistivities of 30 cgs rayls for fresh snow, 60 cgs rayls for a plowed field and 170 cgs rayls for the grass field are in good agreement with values previously reported and listed in table 3.1.1.

CHAPTER IV
SOUND PROPAGATION DURING INVERSION CONDITIONS:
EXPERIMENTAL RESULTS

4.1 Summary of Data

Table 4.1.1 gives dates, times and durations of data acquisition. The locations of each session is also indicated. In total data on eight evenings were acquired at Springbank Airport while thirteen days of data originated from the Vulcan site. This last set of data included a stretch of ten essentially continuous days of data acquisition. This information has been used to investigate the overall tendencies of ground-based or elevated inversions to cause enhancement in sound levels at the surface relative to normal daytime meteorological conditions.

Aside from this long term statistical analysis of the data, several interesting episodes have been looked at more closely, especially those associated with the chinook event of March 1 and 2, 1984, and an attempt made to make theoretical predictions of the excess attenuations using ray tracing analysis. The sometimes large disparity between the measured and theoretical attenuations indicates the potential for further study in this particular area.

Table 4.1.1Data Acquisition Times, Durations and Locations

Date	Start (mst)	Duration (h)	Location
November 5/83	15:10	6.5	Springbank
November 11/83	14:20	5.0	Springbank
November 13/83	17:30	5.0	Springbank
November 17/83	20:50	2.2	Springbank
November 18/83	20:20	2.3	Springbank
November 19/83	15:30	6.8	Springbank
November 26/83	14:20	8.7	Springbank
December 3/83	15:45	6.3	Springbank
February 27/84	14:50	24.8	Vulcan
February 28/84	15:45	25.3	Vulcan
February 29/84	17:45	22.3	Vulcan
March 1/84	16:35	27.2	Vulcan
March 2/84	20:30	17.2	Vulcan
March 3/84	23:25	24.2	Vulcan
March 4/84	23:40	19.8	Vulcan
March 6/84	14:45	27.3	Vulcan
March 16/84	16:30	2.1	Vulcan
March 17/84	05:25	26.3	Vulcan
March 18/84	07:55	25.4	Vulcan
March 19/84	09:25	27.1	Vulcan
March 20/84	12:35	23.5	Vulcan

It is most convenient to present the results in four sections. Section 4.2 concerns the effect of ground-based inversions on short-range sound propagation. In section 4.3 the general effect of ground-based and elevated inversions on the long-range propagation of sound is looked at, while in sections 4.4 and 4.5 specific cases of effects of the nocturnal and elevated inversions respectively are presented.

4.2 The Ground-Based Inversion: Close-Range Effects on the Propagation of Sound

Figures 4.2.1 and 4.2.2 are plots of the measured and theoretical excess attenuations versus frequency for the 300 m and 550 m microphone locations at Springbank Airport. Data at 125 Hz has been excluded because of the poor SNR at this distance and frequency. The same data for the 50 m receiver has already been presented in figure 3.3.1a and b. Figures 4.2.1 and 3.3.1a are for the plowed surface while the other two are for the same surface with a covering of approximately 10 cm of fresh snow.

Clearly at these distances there was no enhancement due to the presence of a ground inversion. In fact the data for the plowed surface would seem to indicate a significant attenuation of 10 dB relative to that predicted at 1000 and 2000 Hz. As wind speeds were always less than 2 m/s at a height of five meters these levels cannot be

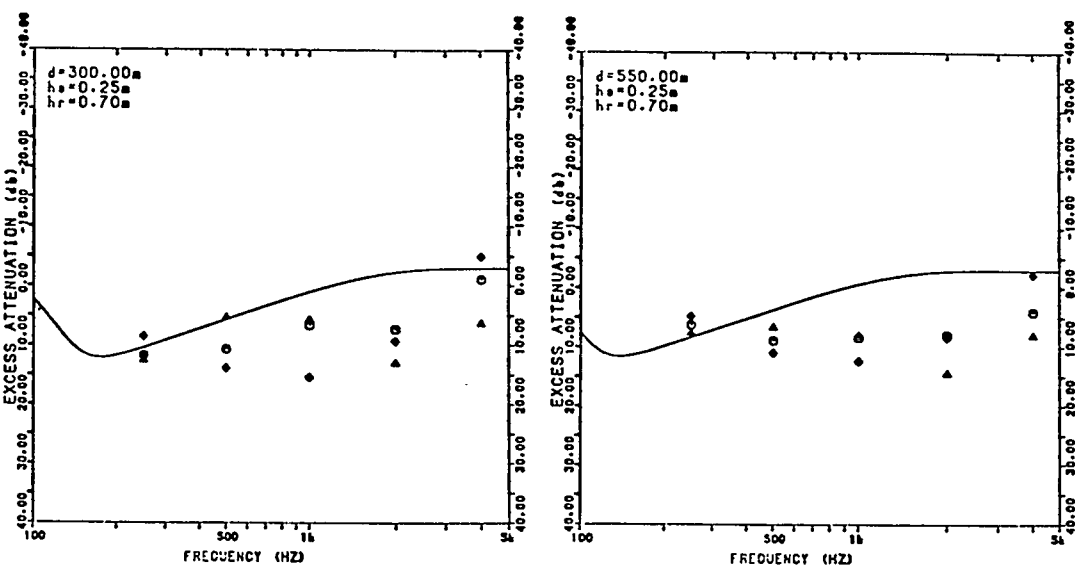


Figure 4.2.1. Measured and theoretical excess attenuations,
 Springbank site (plowed field): $\sigma=60$, $\langle\mu^2\rangle=2 \times 10^{-5}$, $\rho_a=\rho_\delta=0.80$.
 See figure 3.3.1a. for interpretation of symbols.

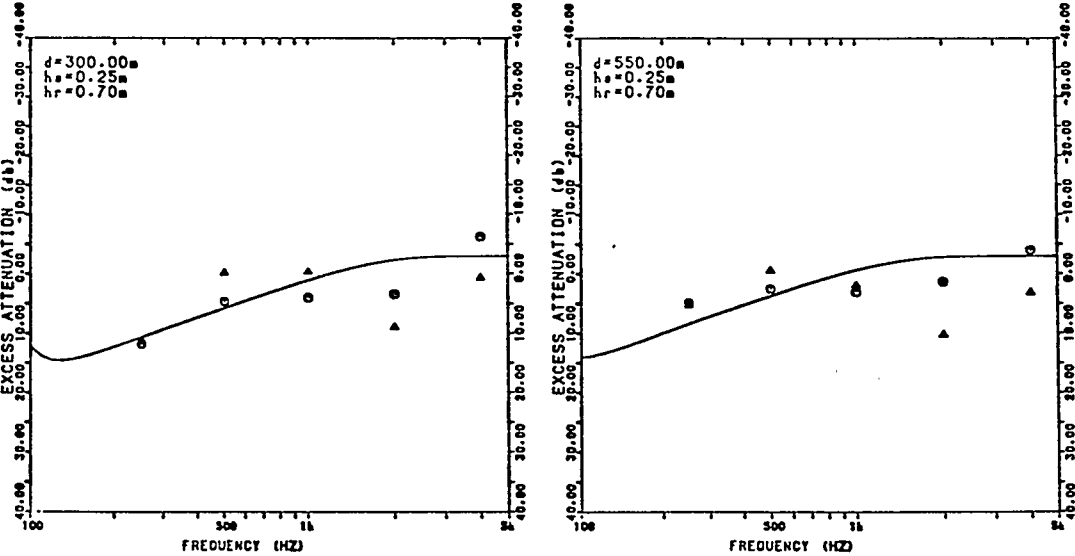


Figure 4.2.2. Measured and theoretical excess attenuations,
 Springbank site (snow-covered): $\sigma=30$, $\langle\mu^2\rangle=2 \times 10^{-5}$, $\rho_a=\rho_\delta=0.80$.
 See figure 3.3.1b. for interpretation of symbols.

explained by refraction effects of wind. It is more plausible that it was in the extreme irregularity of the surface that these seemingly random fluctuations in excess attenuations arose.

The soil cover consisted of clumps of varying sizes, from a few millimeters to tens of centimeters, so the flow resistivity could be expected to vary considerably over a very small surface area. While the fluctuating wind velocity cannot account for the attenuations at these distances it may have been sufficient to shift the point of incidence of the direct sound wave enough that it "saw" a surface of different flow resistivity at different instances of time.

This explanation is strengthened by the considerably better fit of the data to theory for the snow covered surface. The blanket of snow created a much more uniform surface and hence a more uniform and predictable flow resistivity.

In summary, it can be concluded that for source-receiver distances of about 500 m and smaller the refraction of sound caused by ground-based inversions had no discernible effect on sound levels close to the ground. Instead, the attenuations observed are dominated by the ground surface itself.

4.3 The Effect of Temperature Inversions on the Long-Range Propagation of Sound

The continuous operation of the portable monostatic SODAR at the Vulcan site permitted routine classification of different meteorological conditions in the lower 500 m of the boundary layer of the atmosphere. Figure 4.3.1 shows typical sounder records for three atmospheric conditions: a ground inversion, an elevated inversion and thermal plumes arising from the convective rising of warm air on sunny afternoons. Temperature turbulence in the inversion layer or the convective plumes leads to an increased amount of acoustic energy being scattered back towards the sounder. The result is a strong signal (dark record) on the facsimile chart. For a good review of the interpretation of such facsimile records the reader is referred to Brown and Hall (1978).

To investigate the general effect of the nocturnal and elevated inversion on sound propagation near the surface the data was grouped according to the above three types of sounder returns, binned for each frequency and distance into 5 dB wide bins and the results examined. These are presented in figure 4.3.2 and represent 70 hours of data while elevated inversions were evident, 49 hours during ground-based inversions and 24 hours of data acquired

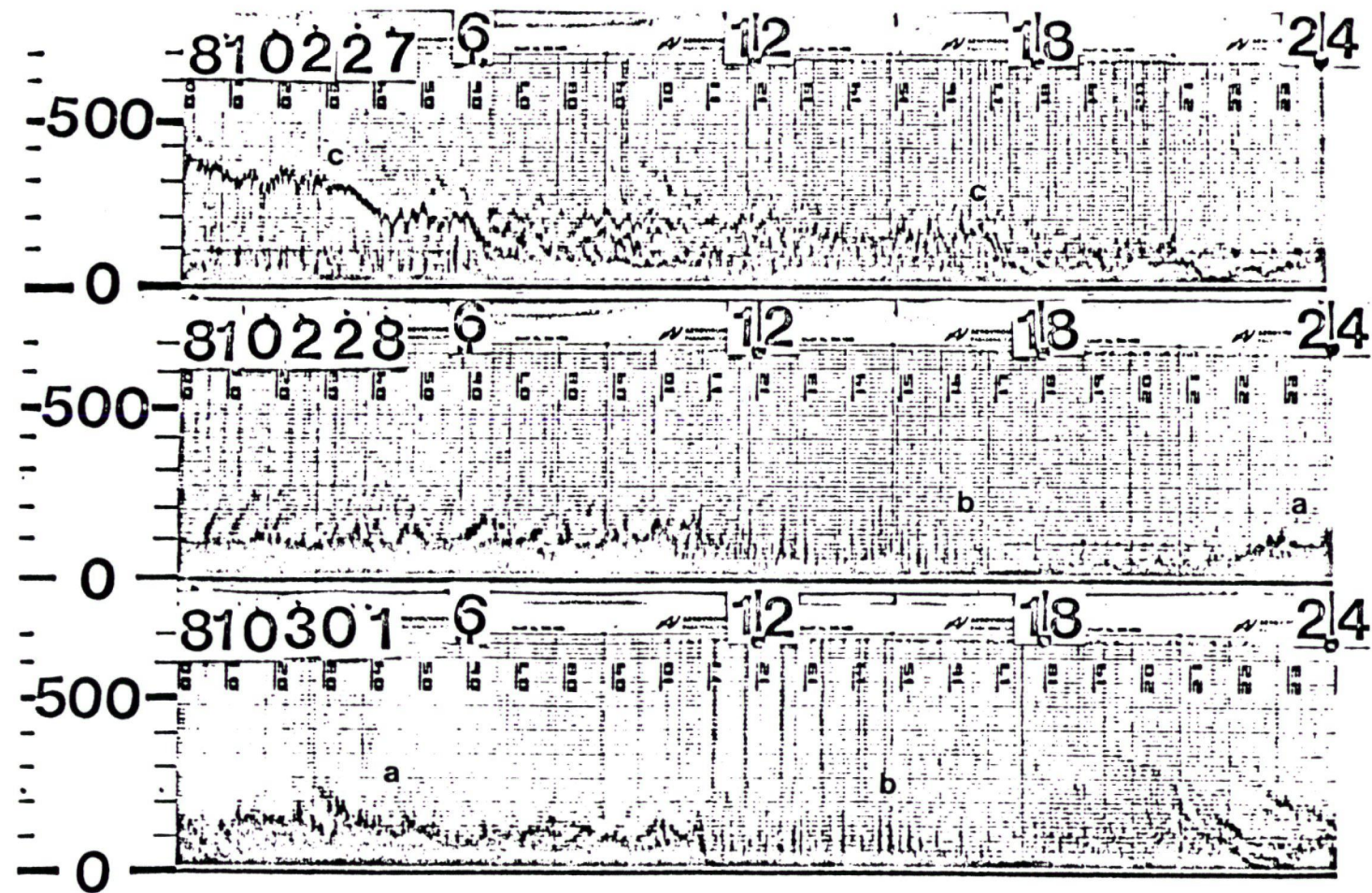


Figure 4.3.1. SODAR records of ground inversions (a), thermal plumes (b) and elevated inversions (c).

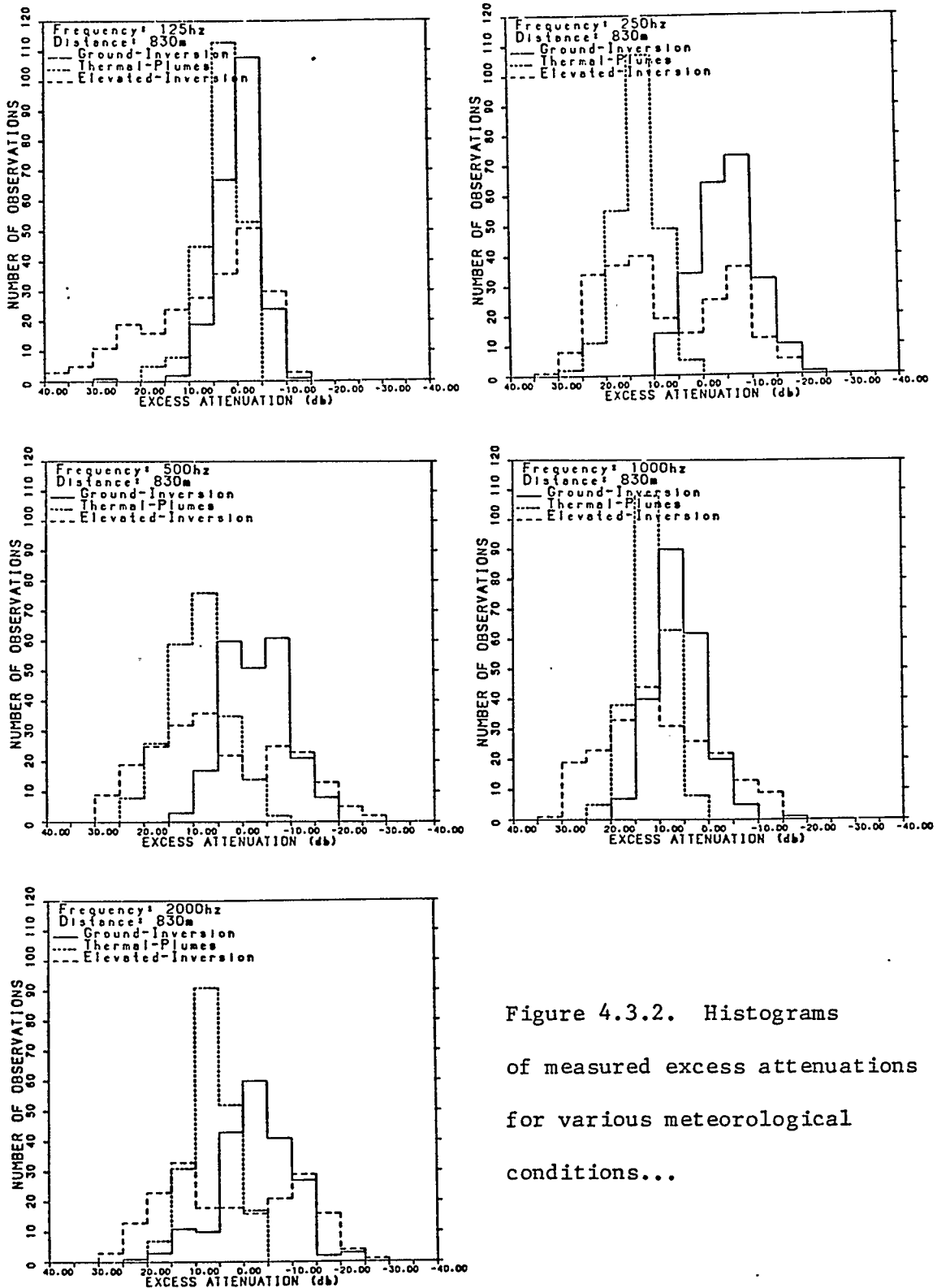


Figure 4.3.2. Histograms
of measured excess attenuations
for various meteorological
conditions...

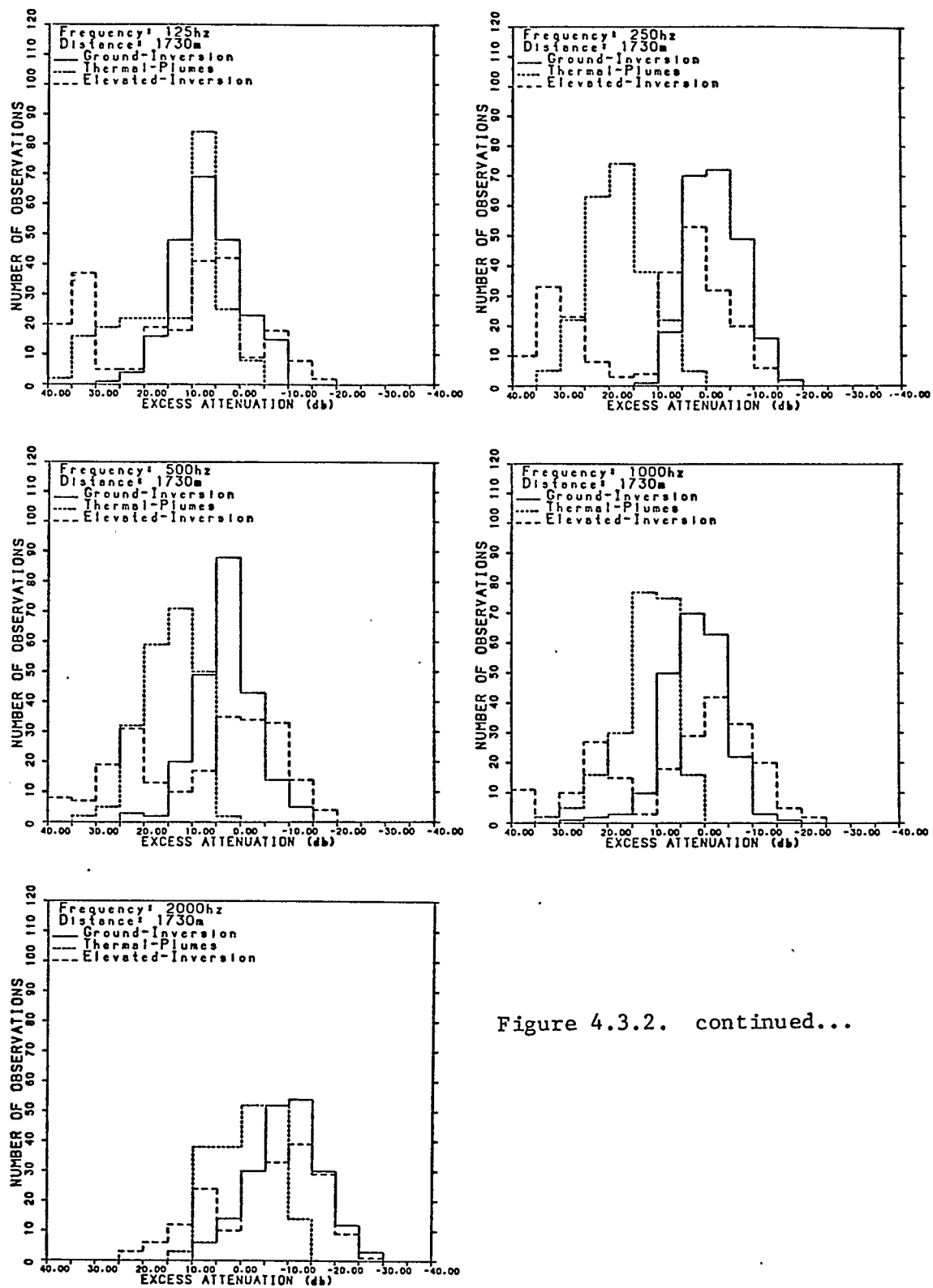


Figure 4.3.2. continued...

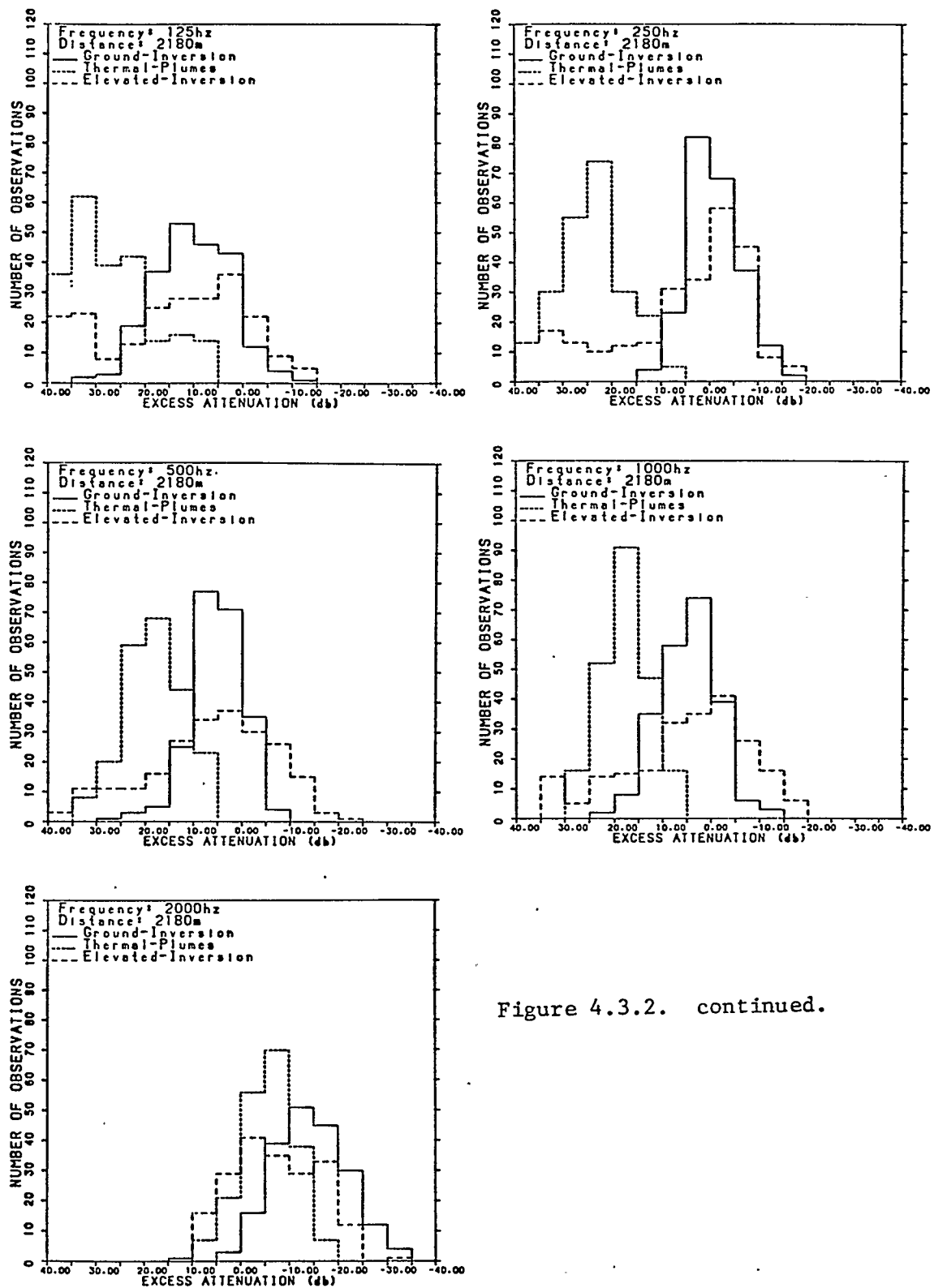


Figure 4.3.2. continued.

during thermal plume activity. The total number of observations for each circumstance have been normalized so that the area under each histogram is the same.

It is immediately seen that at distances of 830 m and beyond there was a significant enhancement of sound levels during ground inversions relative to those during afternoon lapse conditions. The effect increased with distance from the source although this is mainly the result of increasing attenuation with distance during the day; the excess attenuation during ground inversions was remarkably constant with respect to frequency and distance with average excess attenuations varying between -5 and +5 dB. The presence of a nocturnal inversion seemed to have nullified much of the effect of the ground surface.

The data for elevated inversions showed some interesting behavior. At almost every frequency and distance the data formed two peaks: one at a higher attenuation than that for the thermal plume data and the other at a lower attenuation than that occurring during ground-based inversions. This is evidence of the predicted focusing regions and shadow zones discussed in chapter one. As the elevated inversion rose or descended the region where focusing occurred at the surface moved further from or closer to the sound source with sound levels at the surface fluctuating accordingly. This movement of the caustic and

shadow zone resulted in the observed double peak in the measured sound levels.

4.4 The Nocturnal Inversion

Figure 4.4.1 contains plots of excess attenuations versus frequency for four evenings during which ground inversions of various strengths were evident and for which meteorological data was available. The solid lines again represent theoretical attenuations for a flow resistivity of 170 cgs rayls.

Immediately obvious is the disappearance of the shadow zone at all distances. Sound levels at 250 Hz were up to 20 dB higher than predicted. Intensities at 125 Hz tended to be about 10 dB lower than the average of near 0 dB excess attenuation while those at 2000 Hz reached values 18 dB above this.

Temperature inversion strengths in the figure range from $3^{\circ}\text{C}/100\text{ m}$ to $1.5^{\circ}\text{C}/100\text{ m}$ as indicated. Interestingly, there seems to be little correlation between the inversion strength and the excess attenuations. The strongest temperature inversion also had associated with it a large wind gradient of $8.0\text{ m/s}/100\text{ m}$ from source to receiver but still showed no definite enhancement relative to the weakest inversion ($1.5^{\circ}\text{C}/100\text{ m}$ and $1\text{ m/s}/100\text{ m}$ from source to receiver).

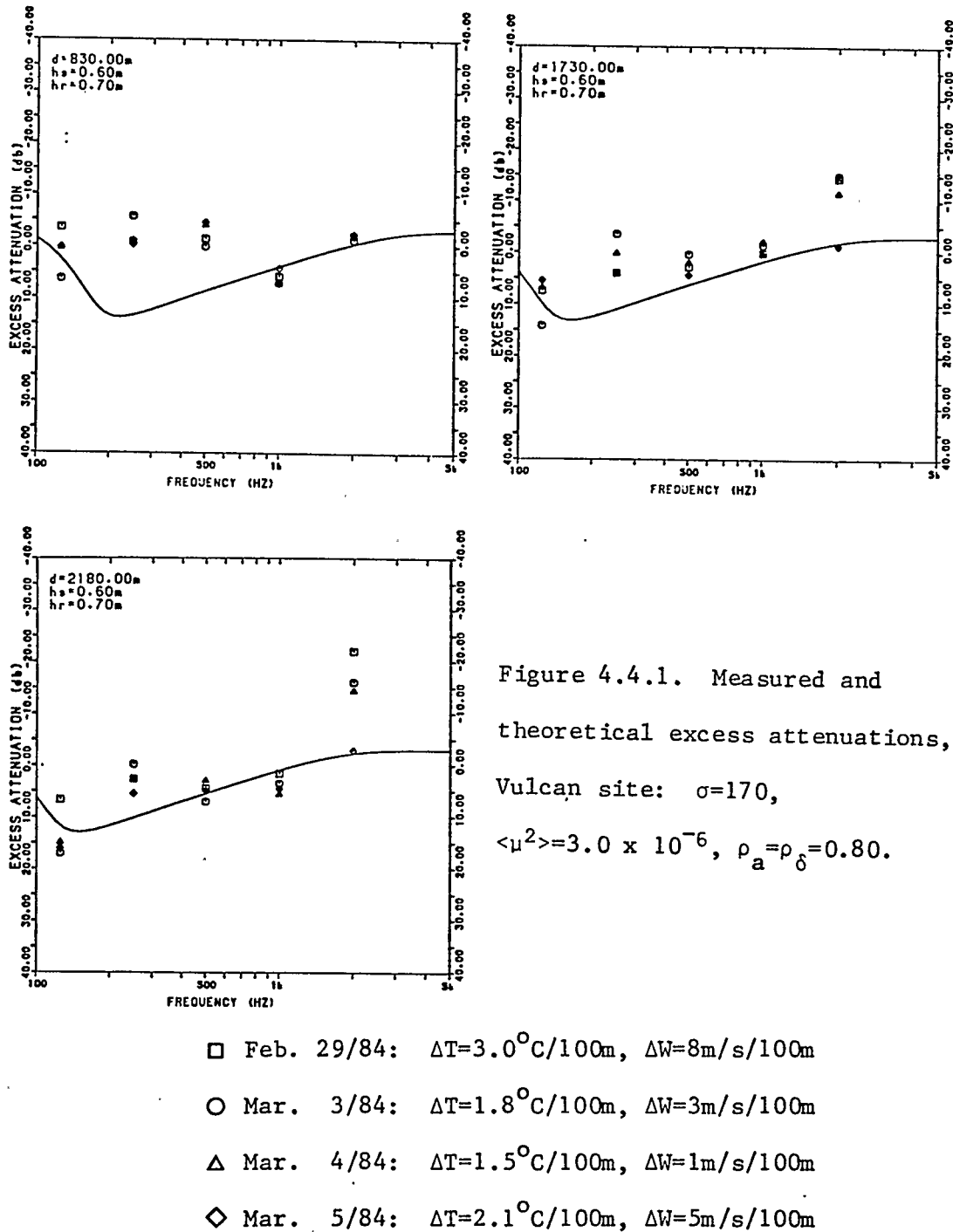


Figure 4.4.1. Measured and theoretical excess attenuations, Vulcan site: $\sigma = 170$, $\langle \mu^2 \rangle = 3.0 \times 10^{-6}$, $\rho_a = \rho_\delta = 0.80$.

Ray tracing analysis for this strong inversion indicates that acoustic rays propagating at elevation angles up to 20° were being refracted back to the surface within 1200 m from the source. The excess attenuations predicted are 2 dB at 830 m, 20 dB at 1730 m and 23 dB at 2180 m. Clearly the latter two are in poor agreement with the measured values. These discrepancies are typical of those seen in the other cases.

Since equations 1.5.2 and 1.5.3 give theoretical values of excess attenuations closer to those measured it seems likely that in the case of the nocturnal inversion ground reflections are of considerable importance in determining the total sound field. The disappearance of the shadow zone is then expected since the effect of the inversion is to decrease θ in equation 1.4.5 so that R_p no longer approaches -1. Essentially it is as if the source and receiver were higher above the surface in which case figures 1.4.4b-e display the effect. Much theoretical work remains to be done in this area.

Finally, figure 4.4.2 is presented to illustrate the typical strong correlation between the appearance and disappearance of the ground-based inversion and the rise and fall of the measured excess attenuations. During the inversion sound levels were, on average, 15 to 20 dB higher than before its development and after its destruction.

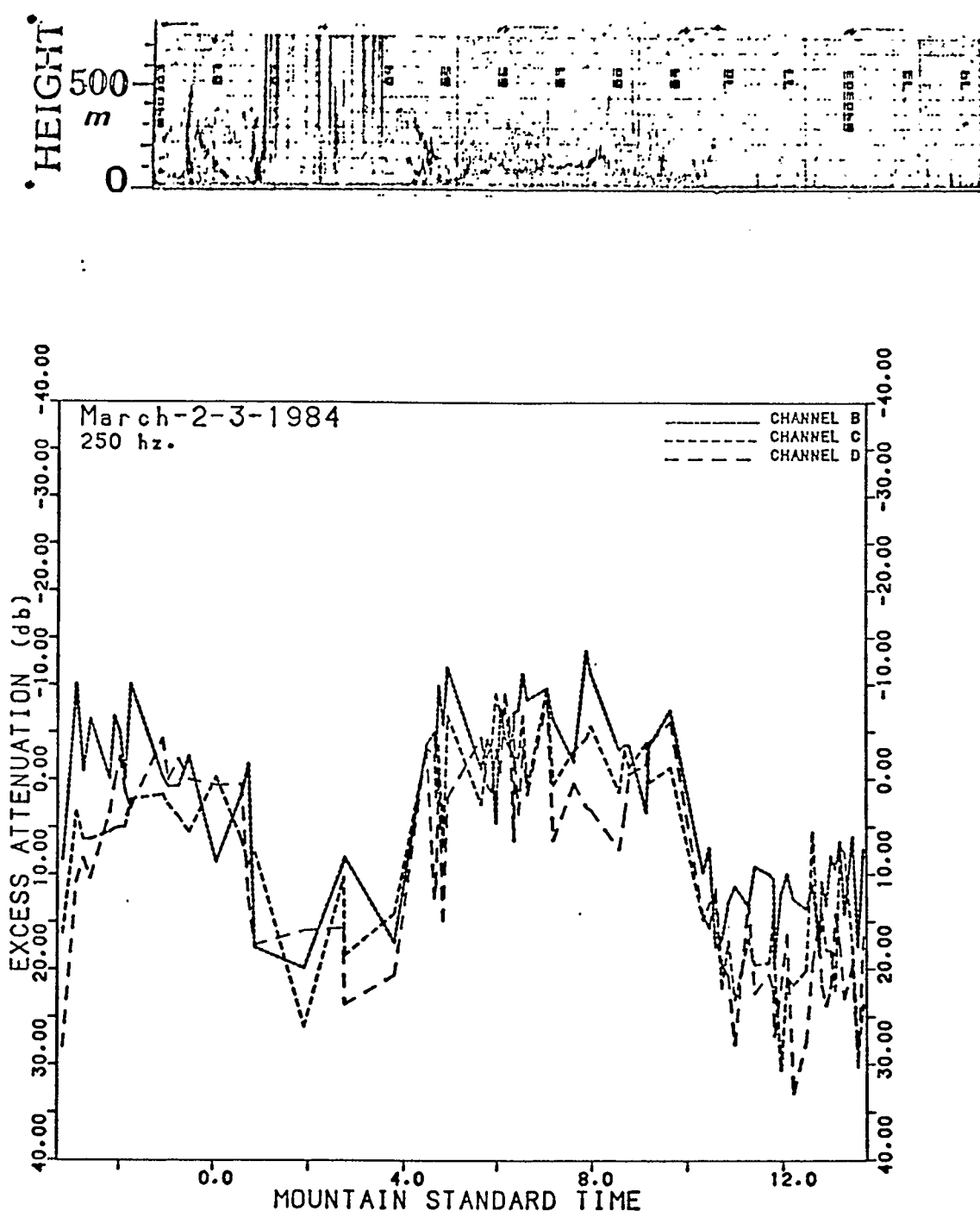


Figure 4.4.2. SODAR record and measured excess attenuations for nocturnal inversion of March 3, 1984 (Vulcan site).

Channel B ≈ 830m, Channel C ≈ 1730m, Channel D ≈ 2180m.

4.5 The Elevated Inversion

Figure 4.5.1 is the monostatic SODAR record of the descent of the chinook layer on March 1 and 2, 1984. In figure 4.5.2 are the recorded excess attenuations at 125 and 250 Hz for approximately the same period of time. Data was qualitatively similar at the other frequencies but somewhat noisier. Tethersonde data of March 2 indicated that the temperature rose approximately 7°C and the westerly component of the wind increased 7.5 m/s in a layer about 100 m thick.

This chinook event proved to be exceptionally good for the experimental study. Not only were the wind and temperature gradients associated with it large enough to produce the desired refraction effects but also the inversion layer was exceedingly slow in descending to the ground, taking well over a day to reach the surface. The height of the layer oscillated from 75 to 300 m during its existence and ground winds were light permitting the observation of several interesting phenomena.

As figure 4.5.2 illustrates sound levels before the initial appearance of the inversion layer at about 1:00 MST on March 1 were extremely low at the two farthest channels. Tethersonde data in the early evening of February 29 indicated a strong easterly wind gradient (increasing wind

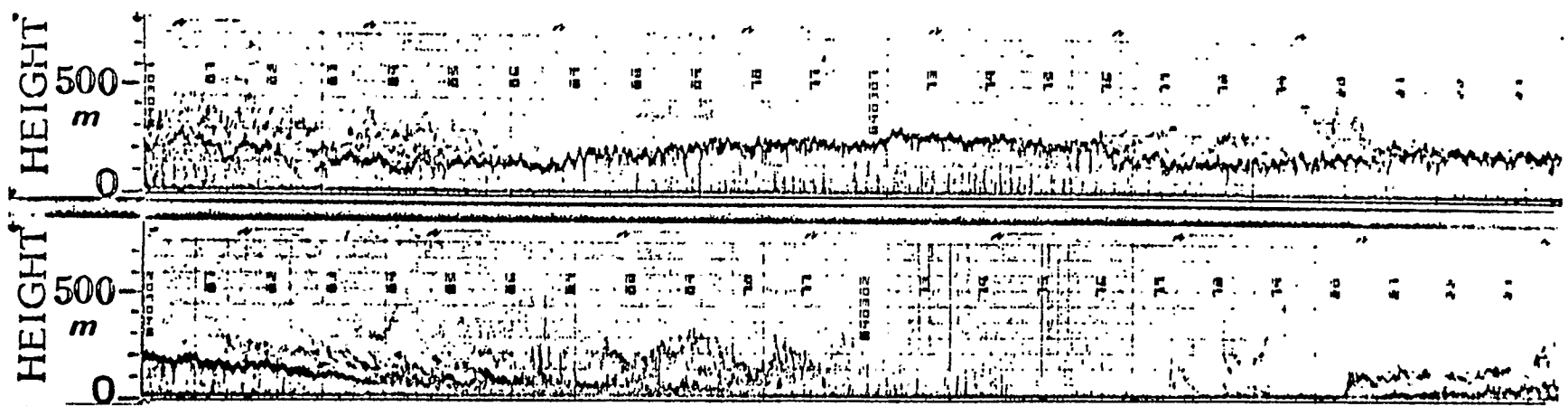


Figure 4.5.1. SODAR record of chinook event of March 1-2, 1984 (Vulcan site).

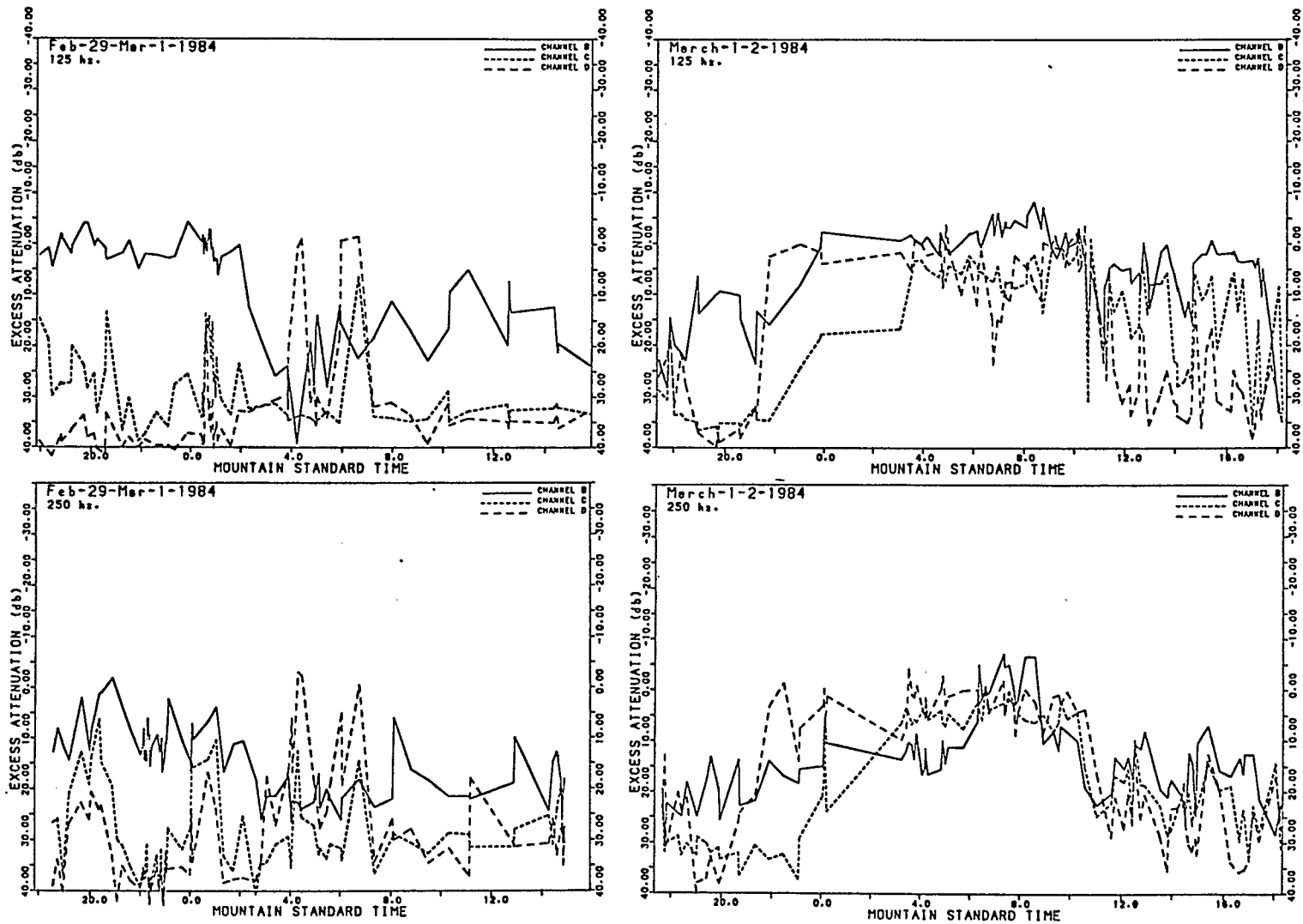


Figure 4.5.2. Measured excess attenuations for Chinook event of March 1-2, 1984 (Vulcan site).

speed with height along a line from the receivers to source) consistent with these measured intensities.

At about 2:00 MST on March 1 the sound level at the 830 m microphone location dropped precipitously as the chinook layer descended to 150 m. Levels at all three channels remained low for the rest of the day except for two brief events shortly after 4:00 MST and 6:30 MST. Here the sound level at the 2180 m receiver suddenly rose more than 30 dB. A smaller increase occurred in the signal at the 1730 m microphone. These events occurred at exactly the same time as the brief descents of the chinook layer seen in figure 4.5.1.

These observations can be explained by the existing meteorological conditions. Using tethersonde data from the afternoon of March 1, ray tracing analysis has been conducted to determine the paths of the acoustic rays. Figure 4.5.3 contains the results. As figure 4.5.3a indicates, no rays reach the ground between 500 m and 1.75 km from the source. However, at 2.0 km focusing does occur. Figure 4.5.3b is a plot of the predicted excess attenuation versus distance. There is a deep shadow zone between 800 and 1750 m where the excess attenuation is predicted to be between 30 and 35 dB. Beyond this range the excess attenuation rises to about -5 dB at 1830 m and +5 dB at 2180 m from the source. While quantitatively the numbers are not accurate qualitative-

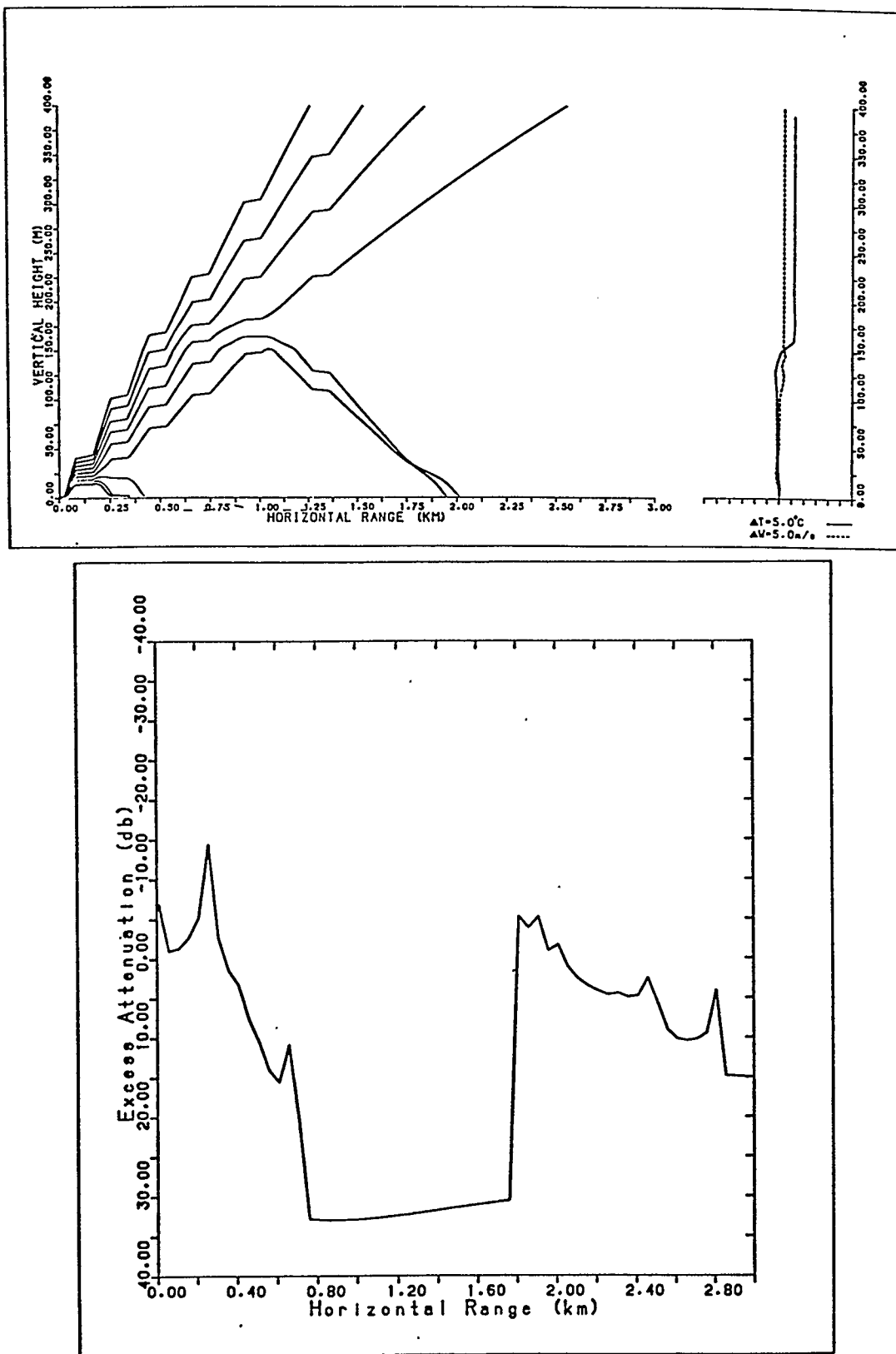


Figure 4.5.3. Ray diagram and theoretical excess attenuations from tethersonde data at 15:40mst March 1, 1984. Elevation angle: $0^\circ - 20^\circ$, 2° increments.

ly the results appear convincing. The sound levels rose and fell at the two farthest microphone locations as the inversion layer descended or ascended causing the boundary of the shadow zone to approach or move further away from the source.

After the above two brief episodes the inversion layer rose somewhat until late in the evening on March 1 when it finally began its final descent to the surface. As this occurred the sound levels rose at every microphone location, reaching maximum values at about 3:00 MST on March 2 and remaining there until approximately 10:00 MST.

Figure 4.5.4 is ray tracing data for tethersonde data acquired at 3:30 MST on March 2. The excess attenuations of 2 dB, -4 dB and -8 dB at 830 m, 1730 m and 2180 m from the source respectively predicted by theory are in reasonable agreement with the measured values.

Shortly after 10:00 MST on the morning of March 2 the inversion layer was destroyed by convective heating near the surface. As this occurred the measured excess attenuations also dropped rapidly, up to 14 dB at 830 m, 18 dB at 1730 m and 24 dB at 2180 m.

As further proof of the cause of the low sound levels recorded during the evening of March 1 before the final descent of the chinook, the inversion layer was artificially raised to a height of 175 m, the actual height

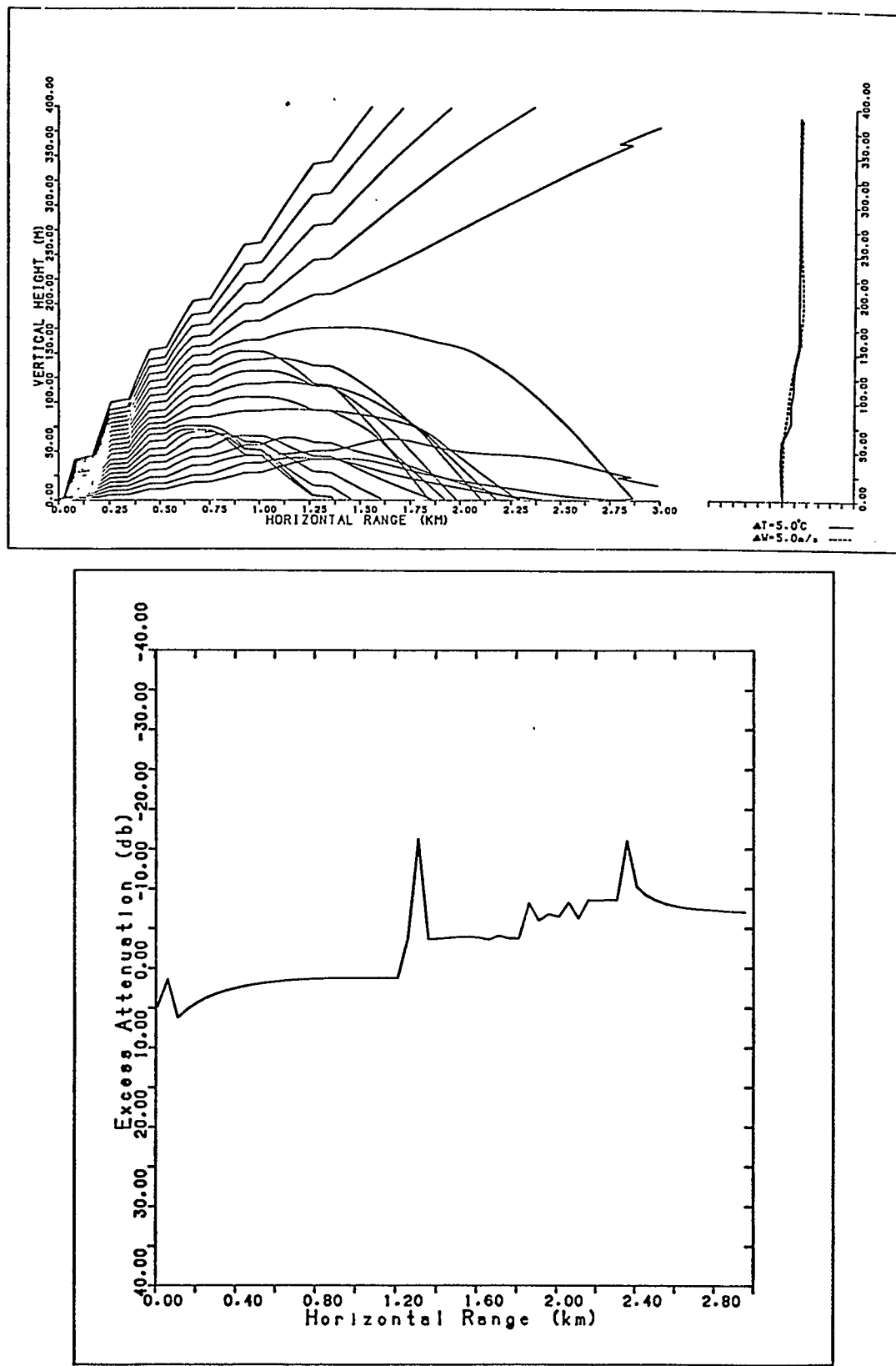


Figure 4.5.4. Ray diagram and theoretical excess attenuations from tethersonde data at 3:30mst March 2, 1984. Elevation angle: $0^\circ - 20^\circ$, 1° increments.

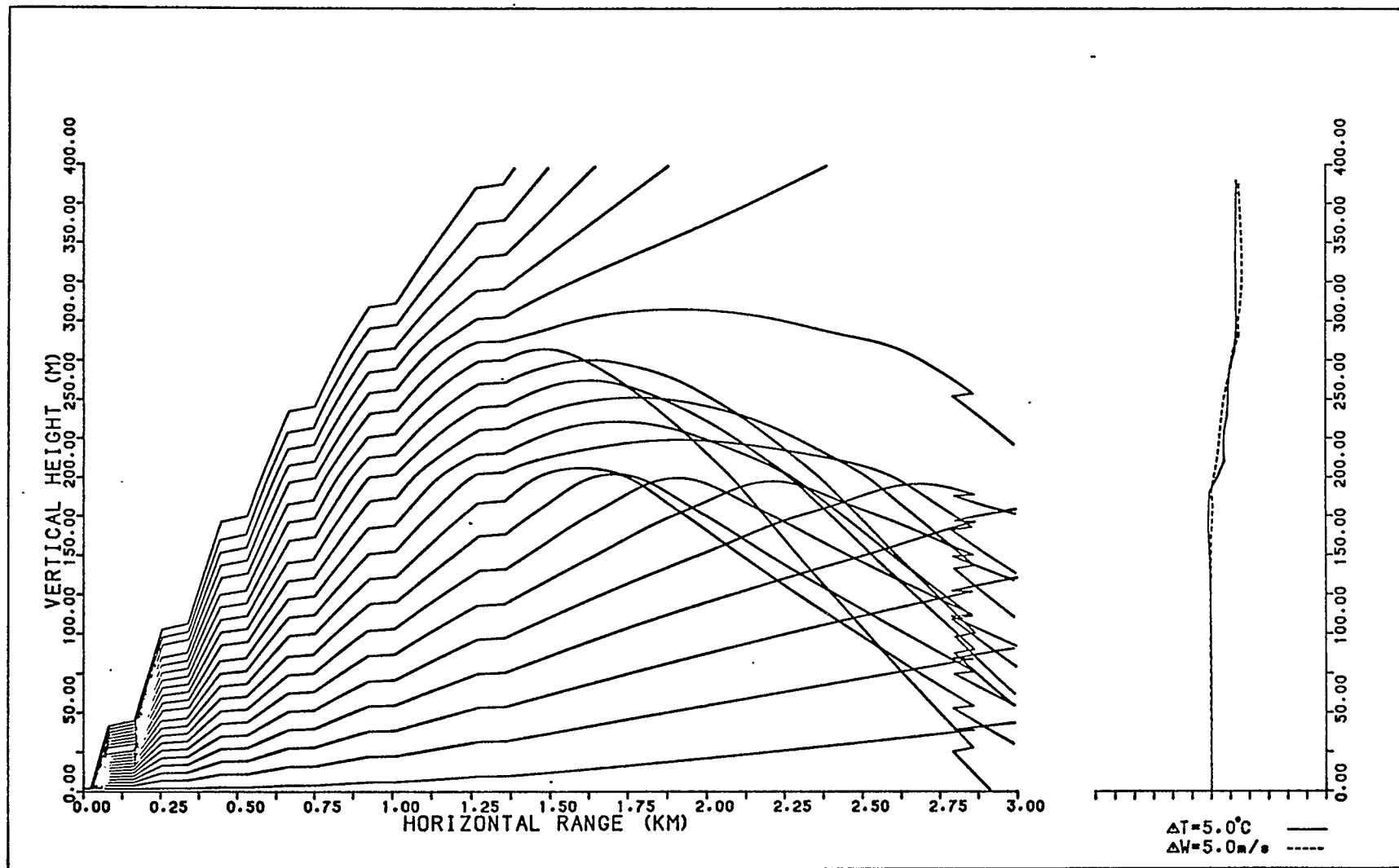


Figure 4.5.5. Ray diagram for artificially raised Chinook layer of March 2, 1984.

of its base at about 20:00 MST. Figure 4.5.5 displays the resulting ray paths. Clearly focusing occurs well outside the range of the most distant microphone located at 2180 m. Of course the structure of the inversion layer is expected to change in the eight hour period separating figures 4.5.5 and 4.5.4. Figure 4.5.5 is nevertheless expected to be a reasonable representation of the actual situation during the evening of March 1.

At least two other occurrences of significant sound level enhancement were observed to be the result of elevated inversions. Figure 4.5.6 are the sounder records for both of these events. Figure 4.5.7 is the record of the excess attenuations in each case.

Between 20:00 MST and 21:00 MST on March 4 multiple layers descended quickly to within 25 m of the surface. Although appearing as a solid ground layer on the facsimile charts, tethersonde data at 22:20 MST clearly indicated a layer from 20 to 120 m in which the temperature rose more than 7°C and westerly winds more than 7 m/s. Ray tracing indicates focusing would occur between 1.0 and 1.25 km from the source while excess attenuations at all three microphone locations would be about -3 dB. These are approximately 5 dB higher than the measured values.

The second event was associated with the complex multi-layer episode of March 19 and 20 shown in

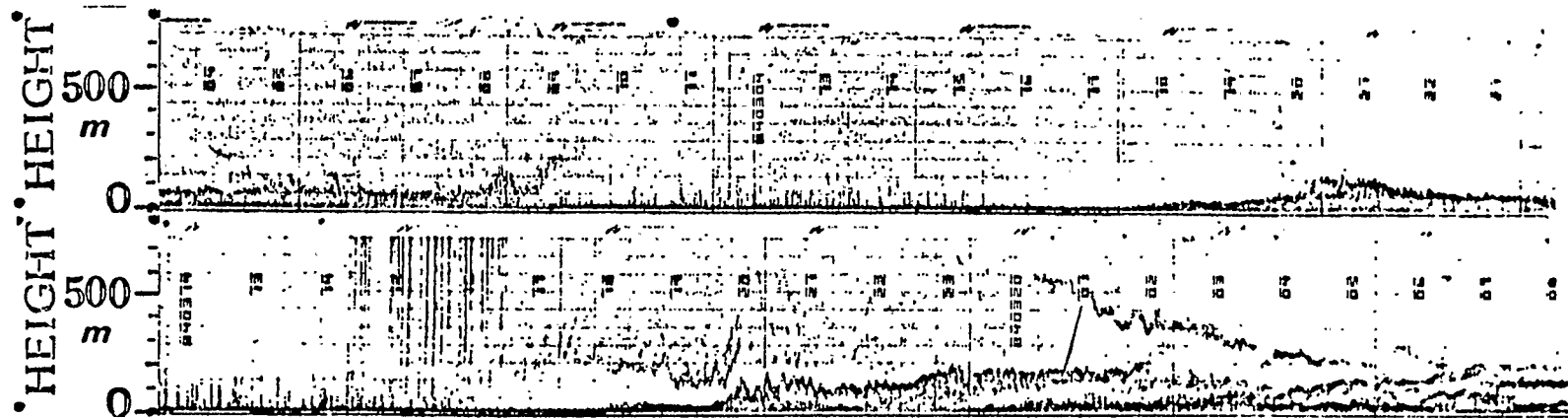


Figure 4.5.6. SODAR records of elevated inversion events of March 4 and 19-20, 1984.

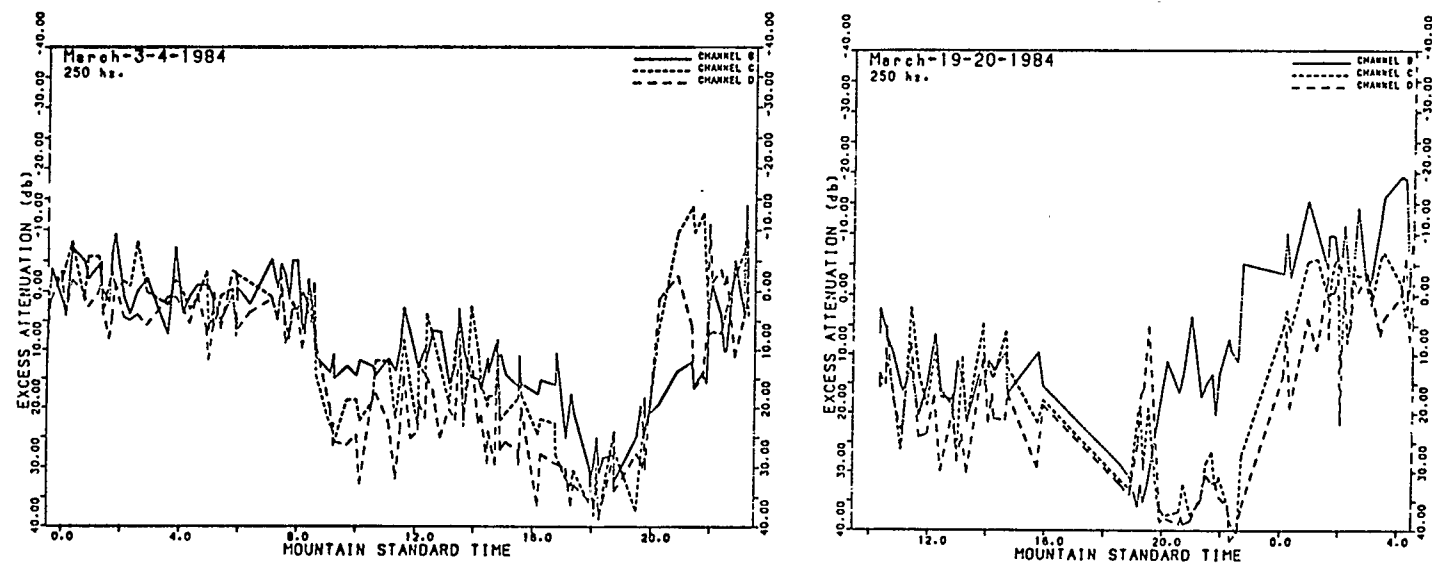


Figure 4.5.7. Measured excess attenuations for elevated inversion events of March 4 and 19-20, 1984.

figure 4.5.6. In this instance the anomalously high sound levels occurred as a result of an ascending layer first seen at 22:00 MST on March 19. As can be seen in figure 4.5.7 sound intensities rose more than 35 dB between 20:00 MST on March 19 and 2:00 MST on March 20. Ray tracing data for tethersonde data acquired at about 00:30 MST on March 20 and again 3:30 MST is presented in figures 4.5.8 and 4.5.9. From the plotted temperature profile one can see that the upper layer at 150 m was actually very weak; temperatures increased only 1°C in its 50 m extent. For the earlier data (figure 4.5.8) most of the downward refraction occurred as a result of a strong wind gradient from source to receiver at the surface to 40 m and a second inversion from 30 m to 70 m in which the temperature rose approximately 3°C. Because these two layers were not at coincident levels no focusing occurred. Instead, the rays were refracted much like they were in the case of a ground-based inversion and it might be expected that the theoretical excess attenuations calculated from ray tracing analysis would be in poor agreement with the actual values as they were in section 4.4. Predicted values are 2, 18 and 24 dB, nearest channel first, while the same attenuations measured in the field were near -5, 3 and 16 dB. The differences are similar to those seen before.

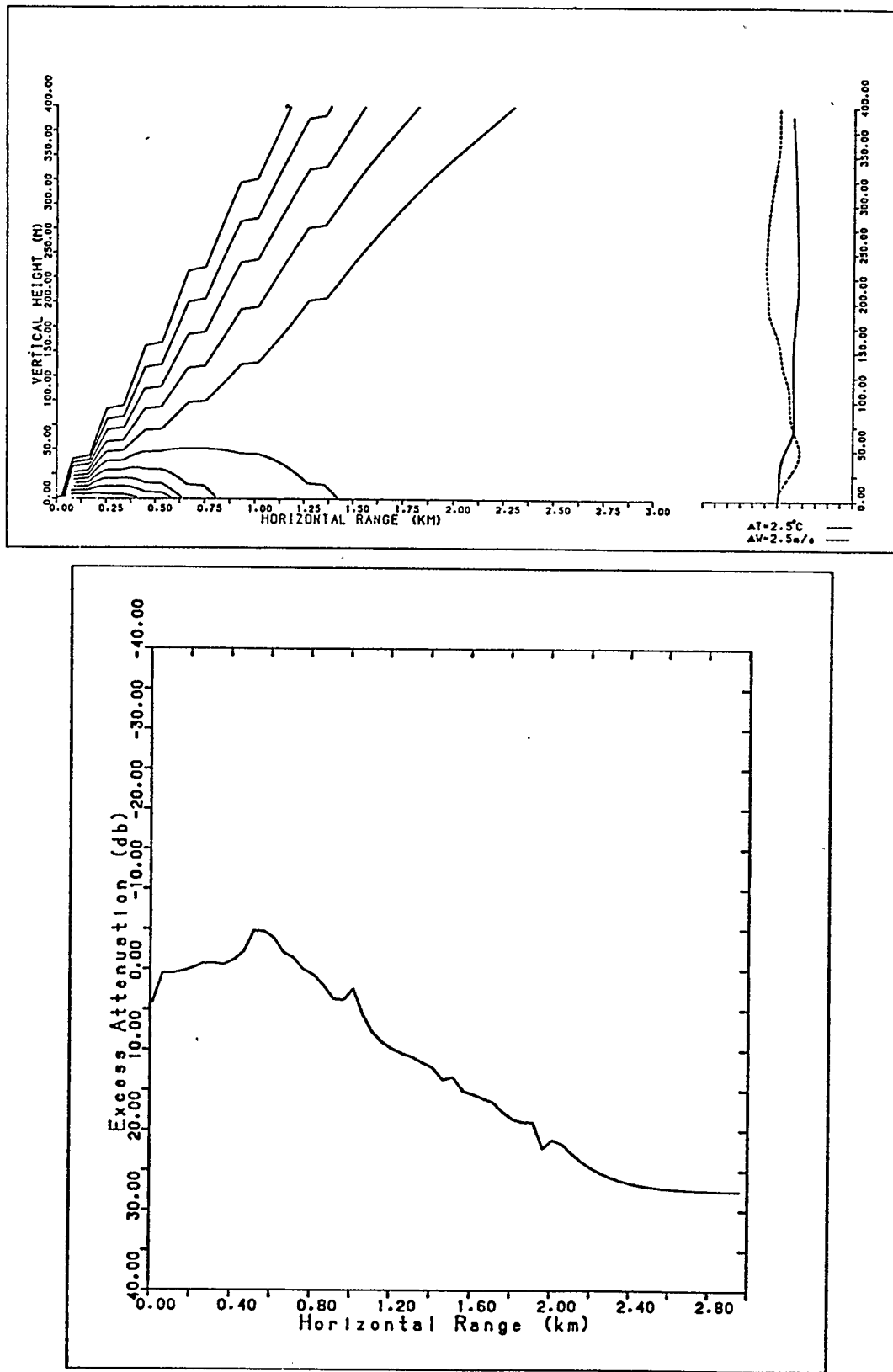


Figure 4.5.8. Ray diagram and theoretical excess attenuations from tethered sonde data at 00:30 mst March 20, 1984. Elevation angle: $0^\circ - 20^\circ$, 2° increments.

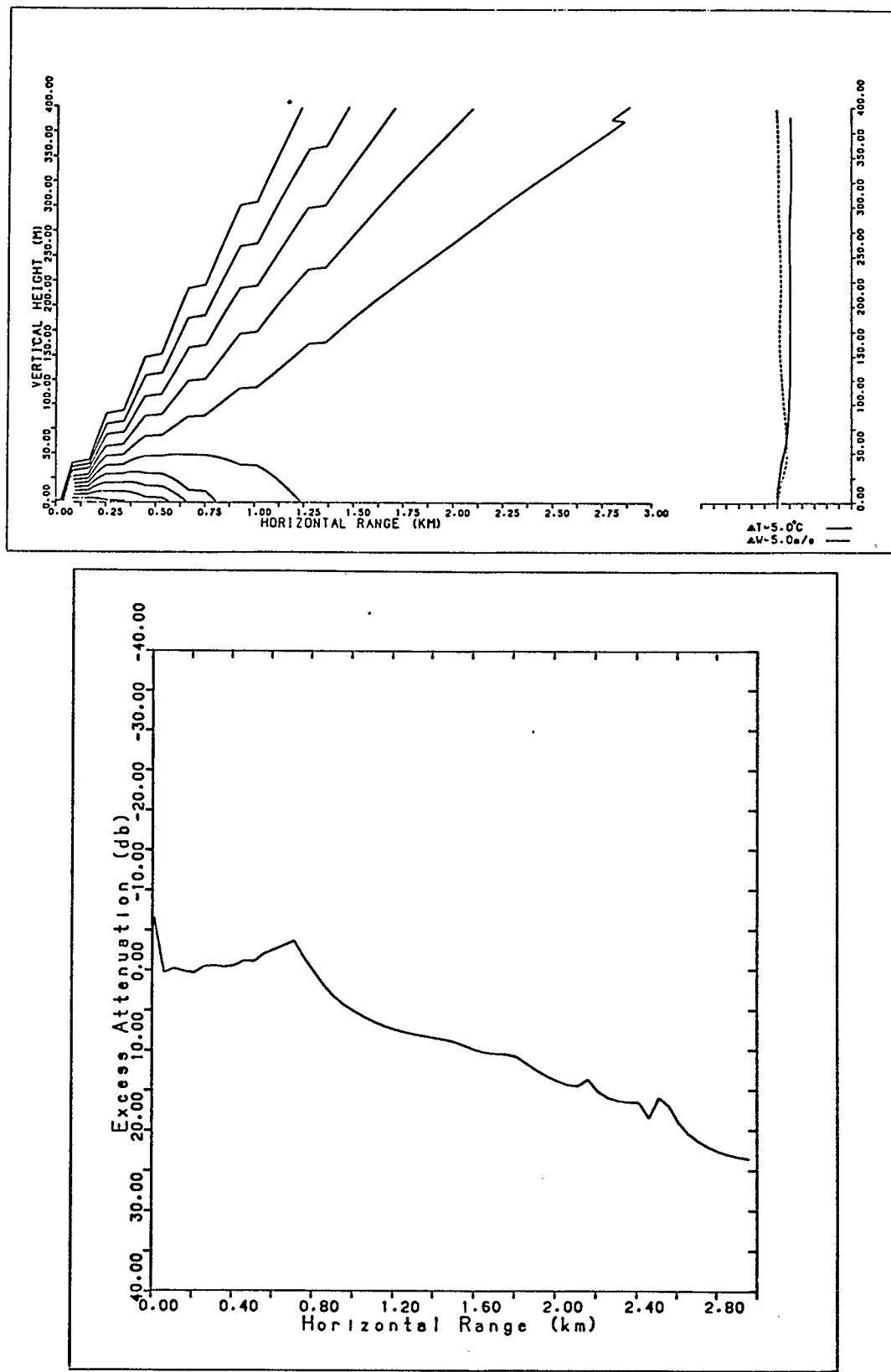


Figure 4.5.9. Ray diagram and theoretical excess attenuations from tethersonde data at 3:30mst March 20, 1984. Elevation angle: $0^\circ - 20^\circ$, 2° increments.

For the later tethersonde data the ray traces in figure 4.5.9 indicate that changes in meteorological conditions in the preceding three hours led to increases in the sound levels of 2 dB at 830 m and 8 dB at 1730 m and 2180 m so that the excess attenuations were only 0, 10 and 14 dB respectively. While these levels are still lower than those recorded in figure 4.5.7 a rise similar to that predicted was seen from 00:00 MST to 3:30 MST.

Excluding the event of March 20 single hop ray tracing analysis seems to provide reasonable estimates of sound levels when elevated inversions are present indicating that ground reflections are not of importance for the ranges studied and that the observed enhancements of sound can be expected to occur over any surface.

CHAPTER V

SUMMARY AND DISCUSSION

5.1 Summary

The major portion of this work was an investigation of sound propagation under inversion conditions in Southern Alberta. It has been found that for distances under one-half a kilometer the sound field due to a point source is determined primarily by the characteristics of the ground surface and by the degree of coherence between the direct and reflected waves as determined by the magnitude of the atmospheric turbulence. For such short-range propagation temperature inversions had no discernible effect on sound levels measured at the surface.

The effect of ground-based and elevated temperature inversions on the measured sound levels for distances between 800 and 2200 m has also been investigated. In this case the presence of a nocturnal inversion was discovered to negate much of the effect of the ground surface resulting in sound levels close to those expected for spherical spreading from a point source. At distances of about two kilometers the sound levels during the night when a ground inversion was present have been found to be up to 25 dB higher than those experienced at the same location dur-

ing a calm, sunny afternoon. Interestingly, the measurements indicated that the enhancement of sound by ground-based inversions is relatively independent of the frequency of the acoustic wave and shows no systematic dependence on the inversion's strength.

Observations of the effect of elevated inversions on sound propagation near the surface verified several phenomena predicted by ray theory. The sound levels recorded far from the source displayed a range of 40 dB for the chinook event of March 1 and 2, 1984. This event consisted of an elevated layer with a temperature gradient of $8^{\circ}\text{C}/100\text{ m}$ and westerly wind gradient of $8\text{ m/s}/100\text{ m}$. Shortly after the layer's appearance on the SODAR chart sound levels dropped 15 dB below normal because of the creation of a shadow zone by the wind and temperature gradients aloft. As the layer descended the focusing region moved into range of the two most distant receivers. The fact that the sound intensities rose simultaneously at each of two microphones at 1730 and 2180 m indicates that this zone of enhancement had a horizontal extent of at least 450 m. Ray tracing analysis using tethersonde data acquired during the chinook event confirmed this conclusion.

Theoretical sound levels obtained using these ray tracing techniques are in reasonable agreement with field measurements in the case of elevated inversions indicating that

reflections from the surface are of only small importance in these situations. In addition, the assumption of incoherent addition of sound intensities where more than one refracted wave is incident on a microphone appears to be valid. Not only are the propagation paths long but the routes followed by two sound rays focusing at a common point may be separated at their apogees by distances of the order of fifty meters. Since turbulence occurs on a scale of approximately one meter any coherence between two such rays will be negligible. There does, however, seem to be a tendency for the theory to predict sound levels slightly higher than those measured. As discussed in the review by Brown and Hall (1978) turbulence can also produce scattering of sound. Such scattering, both forward and backward, will lead to a loss of acoustic energy at the receivers and may explain the observed differences in the measured and theoretical sound levels. In fact the very appearance of the chinook layer on the acoustic sounder record demonstrates that a significant amount of acoustic power is being scattered by turbulence at an angle of 180° to its original direction.

On the other hand ray tracing techniques do not give consistent results for ground-based inversion situations. Reflections from the ground may still be of major importance, although the simple two-path model employed here

does not give good results. A certain degree of coherence is to be expected between the reflected and direct waves since, in this case, path separations are not as great as in the elevated inversion situation. Also, Embleton et al (1976b) have suggested that additional ray paths from source to receiver may contribute to the total sound level. However, the frequency dependence or the strong dependence on the strength of the temperature inversion their theory predicts is not seen. Considerable work remains to be done in this area.

Flow resistivity measurements of three surface types were conducted at two different sites by fitting experimental excess attenuations of sound near the ground to theoretical values predicted by Daigle et al (1978) and Daigle (1979). Values for the flow resistivity of 60 cgs rayls for a plowed field and 30 cgs rayls for the same field with a 10 cm deep covering of snow at Springbank Airport, twenty kilometers west of Calgary, were obtained. In addition a grass field at a second site near Vulcan, Alberta, yielded a flow resistivity of 170 cgs rayls. These values are all in good agreement with previously published results for similar surface types and enabled calculation of the theoretical sound levels with which to compare the measured values in the above investigations.

5.2 Discussion

Throughout this work the effects of inversions on the sound field of a point source have been discussed. While perhaps the easiest with which to make theoretical predictions this is by no means the only type of source in the real world. In general the sound sources that warrant consideration are considerably more extended.

During typical chinook conditions the focusing region for a point source decreases in intensity and increases its distance from the source as the angle between the sound ray and wind shear vectors increases. As a result the region of potential annoyance from high sound levels is relatively small. A more serious situation can occur for a sound source such as a major north-south freeway or railway line. These are better approximated by a line source. In this case there will be an extended focusing region a few kilometers east and running parallel to the source. While the excess attenuations will be similar to those expected from a point source the actual sound intensities will be considerably higher since the levels drop just 3 dB for every doubling of the distance from the source. Naturally, for a more extended source the affected region will be even larger.

Another interesting aspect of the effect of elevated inversions on sound propagation is the spectral content of the enhanced signal. As is the case for any long-range propagation of sound frequencies above 1000 Hz are severely attenuated by atmospheric absorption. For the situation depicted in figure 4.5.4 absorption amounted to a loss of approximately 35 dB at 2000 Hz and over 100 dB at 4000 Hz 2180 m from the source. On the other hand, atmospheric absorption accounted for a loss of only 0.75 dB at 125 Hz and the same distance.

This essentially loss-free propagation of low frequency sound suggests the possibility of long-range effects of elevated inversions on the propagation of infrasound (sound with a frequency under 20 Hz) in the atmosphere. Figure 5.2.1 presents ray diagrams for propagation from a point source on the surface with an elevated layer at heights of 0.5, 1.0, 1.5 and 2.0 kilometers. A wind shear of 10 m/s/100 m and an inversion strength of $10^{\circ}\text{C}/100 \text{ m}$ in a layer 100 m thick has been modeled. Even for an inversion height of 2.0 km refractive focusing occurs within approximately 15 km of the source.

While there are many natural sources of infrasound including thunder (Balachandran, 1979), severe weather systems (Georges, 1973) and meteors (ReVelle, 1980) the most commonly occurring signals are those of the mountain

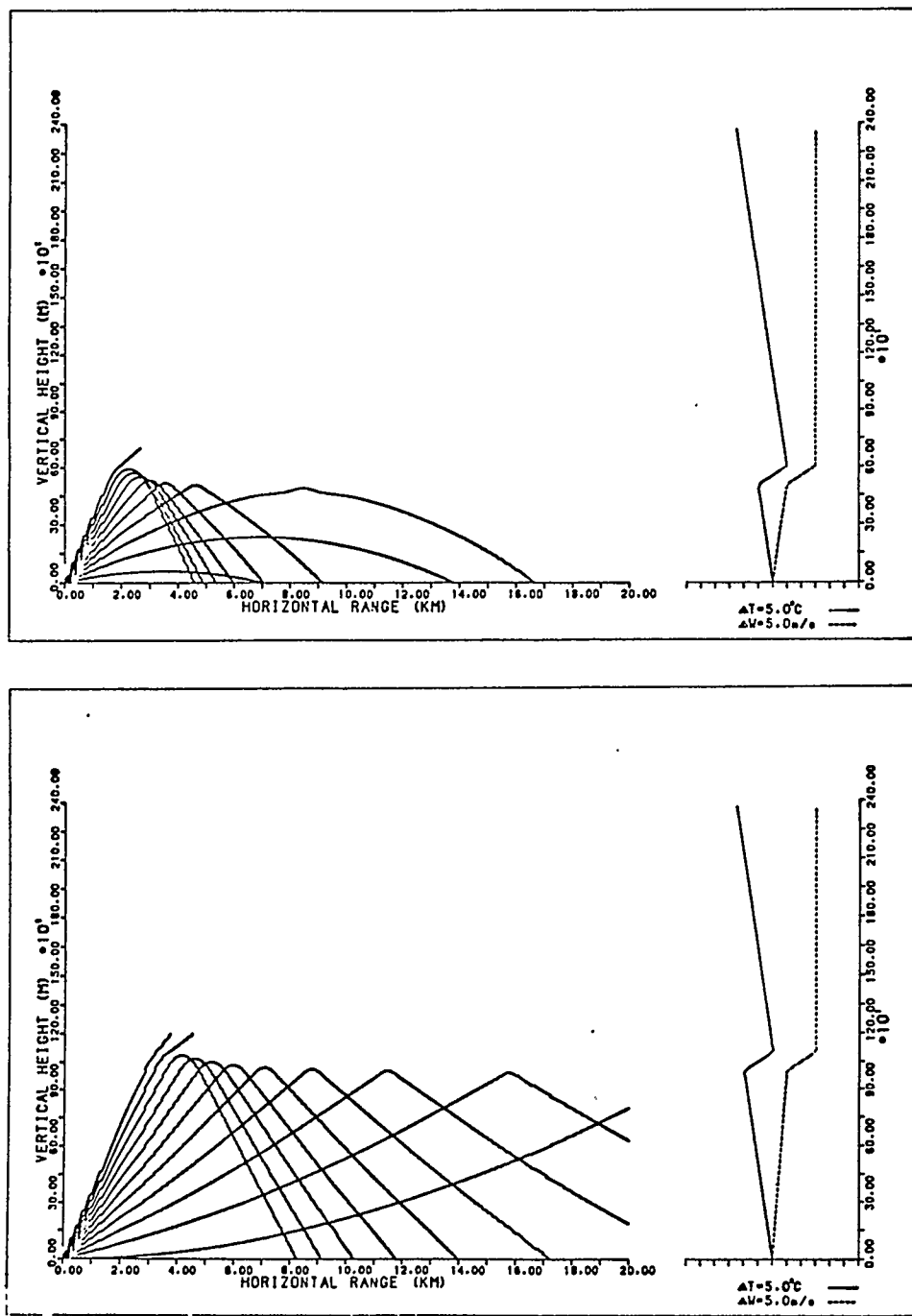


Figure 5.2.1. Theoretical ray paths for 20 Hz infrasound and different inversion heights. Elevation angle: $0^\circ - 20^\circ$, 2° increments.

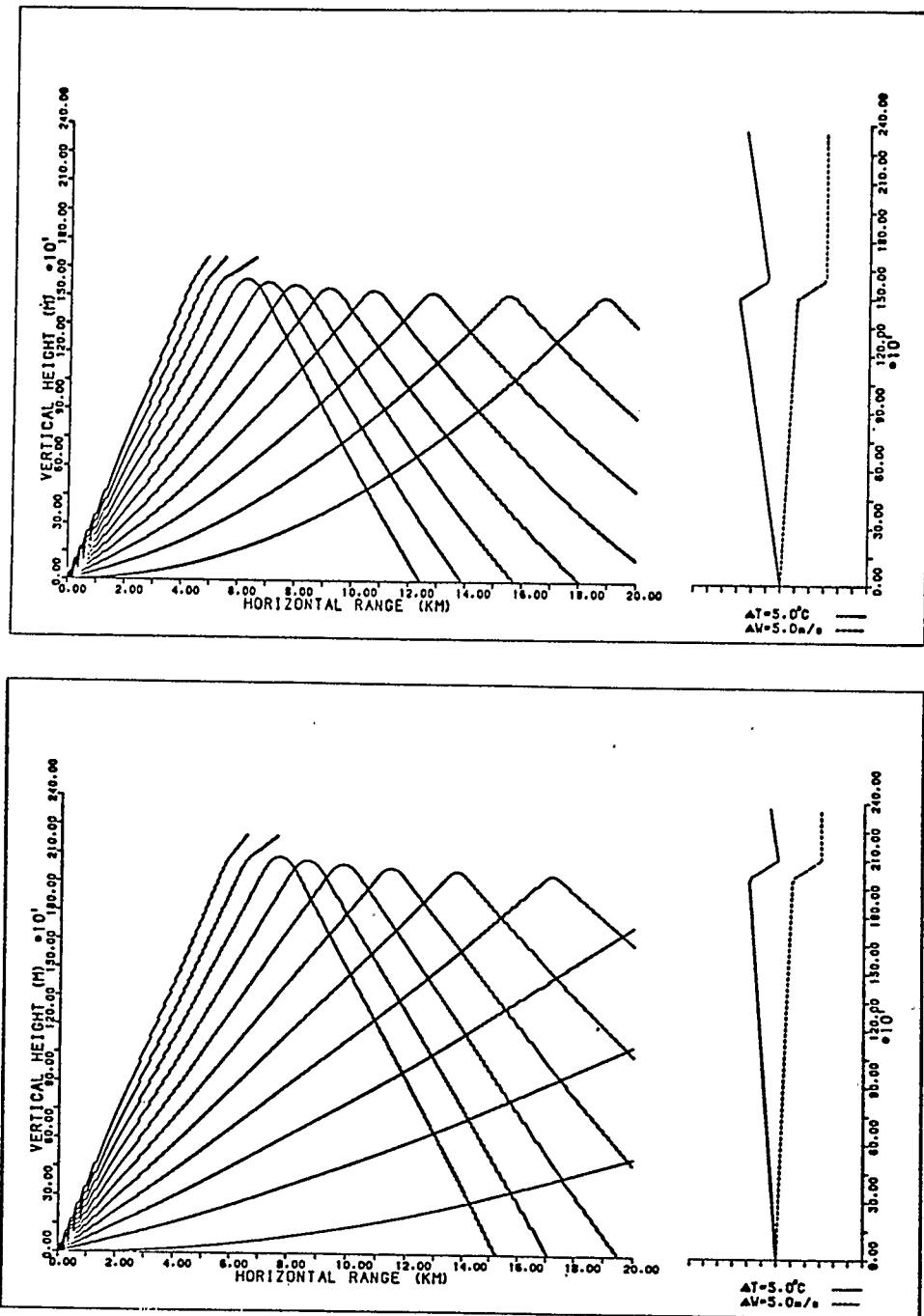


Figure 5.2.1. ...continued.

associated waves. It seems likely that turbulent eddies in the mountain wake are responsible for this infrasound but the exact generation mechanism is not well understood. Suggestions have included dipole and quadrupole generation from airflow systems, vortex shedding and various interactions between the flow and surface such as the production of edge tones. It has been observed that infrasound occurs most frequently when the 500 mb winds are 50 knots or above and from the west. In addition seasonal variations of infrasound occurrences indicate that most signals occur from November to March when mountain lee wave and chinook wind episodes are most prevalent (Bedard, 1978 and references therein).

Calgary's proximity to the Rocky Mountains suggests that infrasound of this nature may be present much of the time. While field measurements to determine if infrasonic waves are enhanced by elevated inversions have yet to be made it has long been known that many people suffer considerable discomfort during chinook events in southern Alberta. Whether or not the effect is psychological or a physical consequence of infrasound is still controversial but this may be indirect evidence for the possible enhancement of ultra-low frequency sound by an elevated inversion.

The greatest enhancement in figure 5.2.1 occurs near the ray that returns to the ground closest to the sound

source. Excess attenuations determined from ray theory for the three highest inversions in the figure range from -4 to -7 dB within 50 to 100 m from this point. Outside this area attenuations quickly approach those expected for spherical spreading from a point source (0 dB). For the inversion at an elevation of 500 m the affected region is considerably larger (>2.0 km) while the excess attenuations vary over a smaller range (-3 to -5 dB). It remains to be seen if focusing of this magnitude is significant.

5.3 Suggestions for Future Work

As is often the case for an experimental investigation the observations give rise to several questions that in turn suggest several areas for further study.

Why does ray tracing analysis give reasonably good predictions of the excess attenuations for elevated inversions but poor values for ground-based inversions? It is probable that reflections from the ground are important in the latter case. An extension of the theory to include possible reflections would be of interest but was beyond the essentially experimental nature of this work.

In the investigation of long-range effects of sound propagation under inversion conditions the ground cover remained relatively unchanged. What effect would different surface types have on the measured sound levels? Differences in

sound intensities over a snow covered surface and those near the same surface in the summer would point quite conclusively to the importance of incorporating reflections into the prediction scheme.

Measurements of the coherence between the different ray paths for various source-receiver geometries are needed to place the theory of propagation of sound in a turbulent medium on a more solid footing. Several investigators have begun such studies (Daigle et al (1983a and b)).

Measurements similar to those carried out in this work, but over much larger distances, perhaps up to 20 km, would be challenging but of considerable interest. On occasion, the bursts from the propane cannon were clearly audible on a neighbouring farm 9 km to the northeast of its location.

Other variations might include studying propagation effects from hilltop to hilltop where ground effects are expected to be minimal, or measuring enhancements over hilltops or barriers of various heights. An elevated source could be used to simulate effects of aircraft as they are taking off or landing. Early theoretical investigations indicate that for elevated inversions the caustics move closer to the region beneath the source as the source height approaches that of the inversion base. Enhancements

are expected to be comparable to those for a source on the ground.

Future study of the effect of inversions on infrasound levels at the earth's surface promises to be one of the most exciting areas of investigation in the next few years. A network of microbarographs and acoustic sounders in southern Alberta could be operated over a period of several years and data analyzed to determine seasonal and daily tendencies in infrasound intensities as well as the correlation between enhanced infrasound signals and the presence of inversions.

BIBLIOGRAPHY

- "Method for Calculation of the Absorption of Sound by the Atmosphere," American National Standard Sl.26-1978.
- N. K. Balachandran, "Infrasonic Signals from Thunder," J. Geophys. Res. 84, 1735-1745 (1979).
- A. Banos Jr., Dipole Radiation in the Presence of a Conducting Half-Space (Pergamon Press, New York, 1966).
- A. J. Bedard, Jr., "Infrasound Originating Near Mountainous Regions in Colorado," J. Appl. Meteor. 6, 1014-1022 (1978).
- L. L. Beranek, Noise and Vibration Control (McGraw-Hill, New York, 1971).
- L. N. Bolen and H. B. Bass, "Effects of Ground Cover on the Propagation of Sound Through the Atmosphere," J. Acoust. Soc. Am. 69, 950-954 (1981).
- L. M. Brekhovskikh, Waves in Layered Media (Academic Press, New York, 1960).
- E. H. Brown and F. F. Hall, Jr., "Advances in Atmospheric Acoustics," Rev. Geophys. Space Phys. 16, 47-110 (1978).
- R. L. Burden, J. D. Faires, and A. C. Reynolds, Numerical Analysis (Prindle, Weber and Schmidt, Boston, 1981).
- L. A. Chernov, Wave Propagation in a Random Medium (McGraw-Hill, New York, 1960).
- C. I. Chessell, "Propagation of Noise Along a Finite Impedance Boundary," J. Acoust. Soc. Am. 62, 825-834 (1977).
- C. I. Chessell, "Meteorological and Ground Effects on the Propagation of Aircraft Noise Close to the Earth's Surface," J. Sound Vib. 60, 251-266 (1978).
- C. F. Chien and W. W. Soroka, "Sound Propagation Along an Impedance Plane," J. Sound Vib. 43, 9-20 (1975).

- C. F. Chien and W. W. Soroka, "A Note on the Calculation of Sound Propagation Along an Impedance Surface," *J. Sound Vib.* 69, 340-343 (1980).
- S. F. Clifford and R. J. Lataitis, "Turbulence Effects on Acoustic Wave Propagation Over a Smooth Surface," *J. Acoust. Soc. Am.* 73, 1545-1550 (1983).
- G. A. Daigle, "Effects of Atmospheric Turbulence on the Interference of Sound Waves Above a Finite Impedance Boundary," *J. Acoust. Soc. Am.* 65, 45-49 (1979).
- G. A. Daigle, T. F. W. Embleton and J. E. Piercy, "Some Comments on the Literature of Propagation Near Boundaries of Finite Acoustical Impedance," *J. Acoust. Soc. Am.* 66, 918-919 (1979).
- G. A. Daigle, T. F. W. Embleton and J. E. Piercy, "Wave Phenomena in Outdoor Sound Propagation," *Physics in Canada*, 39, 85-90 (1983a).
- G. A. Daigle, J. E. Piercy, and T. F. W. Embleton, "Line-of-Sight Propagation Through Atmospheric Turbulence Near the Ground," *J. Acoust. Soc. Am.* 74, 1505-1513 (1983b).
- G. A. Daigle, J. E. Piercy and T. F. W. Embleton, "Effects of Atmospheric Turbulence on the Interference of Sound Waves Near a Hard Boundary," *J. Acoust. Soc. Am.* 64, 622-630 (1978).
- M. E. Delany and E. N. Bazley, "Acoustical Properties of Fibrous Absorbent Materials," *Applied Acoustics*, 3, 105-116 (1970a).
- M. E. Delany and E. N. Bazley, "Monopole Radiation in the Presence of an Absorbing Plane," *J. Sound Vib.* 13, 269-279 (1970b).
- P. J. Dickinson, "Temperature Inversion Effects on Aircraft Noise Propagation," *J. Sound Vib.* 47, 438-443 (1976).
- R. J. Donato, "Propagation of a Spherical Wave Near a Plane Boundary with a Complex Impedance," *J. Acoust. Soc. Am.* 60, 34-39 (1976).
- T. F. W. Embleton, "Sound Propagation Outdoors - Improved Prediction Schemes for the 80's," *Noise Control Eng.* 18, 30-39 (1982).

- T. F. W. Embleton, J. E. Piercy and N. Olson, "Outdoor Sound Propagation Over Ground of Finite Impedance," *J. Acoust. Soc. Am.* 59, 267-277 (1976a).
- T. F. W. Embleton, G. J. Thiessen and J. E. Piercy, "Propagation in an Inversion and Reflections at the Ground," *J. Acoust. Soc. Am.* 59, 278-282 (1976b).
- R. N. Foss, "Effects of Wind and Ground Plane Attenuation on Sound Propagation Near the Ground," *J. Acoust. Soc. Am.* 66, 1088-1092 (1979).
- T. M. Georges, "A Program for Calculating Three-Dimensional Acoustic-Gravity Ray Paths in the Atmosphere," National Oceanic and Atmospheric Administration Technical Report ERL 212-WPL 16 (1971).
- T. M. Georges, "Infrasound from Convective Storms: Examining the Evidence," *Rev. Geophys. Space Phys.* 11, 571-594 (1973).
- D. Habault, "Sound Propagation Over Ground: Analytical Approximations and Experimental Results," *J. Sound Vib.* 79, 551-560 (1981).
- D. Habault and P. J. T. Filippi, "Ground Effect Analysis: Surface Wave and Layer Potential Representations," *J. Sound Vib.* 79, 529-550 (1981).
- U. Ingard, "On the Reflection of a Spherical Sound Wave from an Infinite Plane," *J. Acoust. Soc. Am.* 23, 329-335 (1951).
- U. Ingard, "A Review of the Influence of Meteorological Conditions on Sound Propagation," *J. Acoust. Soc. Am.* 25, 405-411 (1953).
- U. Ingard and G. C. Maling Jr., "On the Effect of Atmospheric Turbulence on Sound Propagated Over Ground," *J. Acoust. Soc. Am.* 35, 1056-1058 (1963).
- R. M. Jones and J. J. Stephenson, "A Versatile Three-Dimensional Ray Tracing Computer Program for Radio Waves in the Ionosphere," Office of Telecommunications Report 75-76 (1975).
- B. A. de Jong, A. Moerkerken and J. D. van der Toorn, "Propagation of Sound Over Grassland and Over an Earth Barrier," *J. Sound Vib.* 86, 23-46 (1983).

- T. Kawai, T. Hidaka and T. Nakajima, "Sound Propagation Above an Impedance Boundary," *J. Sound Vib.* 83, 125-138 (1982).
- L. E. Kinsler and A. R. Frey, Fundamentals of Acoustics (Wiley, New York, 1962).
- R. B. Lawhead and I. Rudnick, "Acoustic Wave Propagation Along a Constant Normal Impedance Boundary," *J. Acoust. Soc. Am.* 23, 546-549 (1951).
- T. Mathews, "A Study of the Propagation of Sound Under Inversion Conditions in Southern Alberta," Report On Work Done Under NSERC Strategic Grant No. G.1075 (1982).
- P. H. Parkins and W. E. Scholes, "The Horizontal Propagation of Sound From a Jet Engine Close to the Ground, at Radlett," *J. Sound Vib.* 1, 1-13 (1964).
- P. H. Parkins and W. E. Scholes, "The Horizontal Propagation of Sound From a Jet Engine Close to the Ground, at Hatfield," *J. Sound Vib.* 2, 353-374 (1965).
- J. E. Piercy, T. F. W. Embleton and L. C. Sutherland, "Review of Noise Propagation in the Atmosphere," *J. Acoust. Soc. Am.* 61, 1403-1418 (1977).
- K. B. Rasmussen, "Sound Propagation Over Grass Covered Ground," *J. Sound Vib.* 78, 247-255 (1981).
- D. O. ReVelle, "On Meteor-Generated Infrasound," *J. Geophys. Res.* 81, 1217-1230 (1976).
- I. Rudnick, "The Propagation of an Acoustic Wave Along a Boundary," *J. Acoust. Soc. Am.* 19, 348-356 (1947).
- I. Rudnick, "Propagation of Sound in the Open Air," in Handbook of Noise Control, C. M. Harris, ed. (McGraw-Hill, New York, 1957), 3-1 to 3-17.
- R. H. Talaske, "The Acoustic Impedance of a Layered Forest Floor," Final Report to U.S. Department of Agriculture Forest Service (1980).
- Sven-Ingvar Thomasson, "Reflection of Waves from a Point Source by an Impedance Boundary," *J. Acoust. Soc. Am.* 59, 780-785 (1976).

Sven-Ingvar Thomasson, "Sound Propagation Above a Layer With a Large Refraction Index," J. Acoust. Soc. Am. 61, 659-674 (1977).

G. Tyras, Radiation and Propagation of Electromagnetic Waves (Academic Press, New York, 1969).

J. R. Wait, Electromagnetic Waves in Stratified Media (Macmillan, New York, 1962).

A. R. Wenzel, "Propagation of Waves Along an Impedance Boundary," J. Acoust. Soc. Am. 55, 956-963 (1974).

F. M. Wiener and D. N. Keast, "Experimental Study of the Propagation of Sound Over Ground," J. Acoust. Soc. Am. 31, 724-733 (1959).

APPENDIX A

EFFECTS OF ATMOSPHERIC TURBULENCE ON THE INTERFERENCE OF SOUND WAVES

In figure 1.4.1 the sound field at R is given by equations 1.4.16 to 1.4.18. This can be rewritten as

$$\Phi = \frac{A_1}{r_1} \exp\{i(k_1 r_1 - \omega t)\} + Q \frac{A_2}{r_2} \exp\{i(k_2 r_2 - \omega t)\} \quad A.1$$

where A_1 , A_2 , k_1 and k_2 are, in the presence of turbulence, the fluctuating amplitudes of the direct and reflected waves and the corresponding fluctuating wavenumbers respectively. All other terms are as defined in section 1.4.

Daigle (1979) set $A_1 = 1 + a_1$, $A_2 = 1 + a_2$
 $k_1 r_1 = k r_1 + \delta_1$ and $k_2 r_2 = k r_2 + \delta_2$ where k is the wavenumber when there is no turbulence present. For time averages (denoted $\langle x \rangle$) over a large number of turbulent fluctuations $\langle a_1 \rangle = \langle a_2 \rangle = \langle \delta_1 \rangle = \langle \delta_2 \rangle = 0$. The mean square sound pressure is then

$$\bar{p}^2 = \frac{A_1^2}{r_1^2} + |Q|^2 \frac{A_2^2}{r_2^2} + \frac{2|Q|A_1A_2}{r_1r_2} \cos\{k(r_2 - r_1) + \gamma + (\delta_2 - \delta_1)\} \quad A.2$$

where $Q = |Q| e^{i\gamma}$

Assuming $\langle a_1^2 \rangle = \langle a_2^2 \rangle = \langle a^2 \rangle$ and that a , δ_2 and δ_1 are normally distributed with standard deviations of $\langle a^2 \rangle$, σ_2 and σ_1 respectively it can be shown that

$$\begin{aligned} \langle \bar{p}^2 \rangle &= \frac{2}{r_1 r_2} \left[\frac{\langle a^2 \rangle}{2} \left(\frac{r_2}{r_1} + |Q|^2 \frac{r_1}{r_2} \right) + \frac{r_2}{2r_1} \left(1 - |Q| \frac{r_1}{r_2} \right)^2 \right. \\ &\quad \left. + |Q| + |Q|(1 + \langle a^2 \rangle \rho_a) \cos(\phi + \zeta) \exp[-\sigma_1^2 (1 - \rho_\delta)] \right] \end{aligned} \quad A.3$$

where $\phi = k(r_2 - r_1)$ and use has been made of the fact that $\langle \cos(\phi + \gamma + \delta_2 - \delta_1) \rangle = \cos(\phi + \delta) \exp[-\sigma_1^2 (1 - \rho_\delta)]$ (see Daigle et al, 1978). Here ρ_δ and ρ_a are the phase and amplitude covariances. This is equation 1.5.2

To compare measured sound levels with those predicted by equation A.3 one must obtain the dependences of $\langle a^2 \rangle$, ρ_a , ρ_δ and σ_1^2 on measurable quantities such as distance, frequency and the strength and scale of wind and temperature fluctuations.

Assuming homogeneous isotropic turbulence where the fluctuating acoustical index of refraction, written $n = 1 + \mu (\mu \ll 1)$, has a spatial correlation function of Gaussian form (Chernov, 1960), $\langle \mu_1 \mu_2 \rangle = \langle \mu^2 \rangle \exp(-\xi^2/L^2)$,

Daigle et al (1978) demonstrate that

$$\sigma_1^2 = \frac{1}{2}(I_1 + I_2)$$

$$\langle a^2 \rangle \approx \frac{I_1 - I_2}{2 + 33/12(I_1 - I_2)} \quad I_1 - I_2 \leq 2$$

$$\langle a^2 \rangle = 0.27 \{ \frac{1}{2}(I_1 - I_2) \}^{0.33} \quad I_1 - I_2 > 2$$

$$\rho_a = \rho_\delta = \frac{L}{1} \int_0^{1/L} \exp(-u^2) du$$

where l is chosen to be one-half the maximum path separation of the direct and reflected waves and

$$I_1 = \sqrt{\pi} \langle \mu^2 \rangle k^2 r_1 L$$

$$I_2 = \frac{I_1}{\Delta^2(\Omega + 1)\sqrt{8\Omega}} \left[\frac{\Delta\Omega}{2} \ln \left(\frac{1 + \Delta\sqrt{2\Omega}}{1 - \Delta\sqrt{2\Omega}} \right) + \tan^{-1} \left(\frac{\Delta\Omega}{1 - \Delta\sqrt{2\Omega}} \right) + \tan^{-1} \left(\frac{\Delta\Omega}{1 + \Delta\sqrt{2\Omega}} \right) \right]$$

with $\Omega = (1 + 1/\Delta^2)^{-1}$ and $\Delta = r_1/kL^2$.

The authors made extensive meteorological measurements

to determine L, the scale of the turbulence, and $\langle \mu^2 \rangle$. They indicate L=1.1 m as a best estimate and measure values of $\langle \mu^2 \rangle$ ranging from 4.8×10^{-6} to 10.8×10^{-6} .